"The ability to perceive or think differently is more important than the knowledge gained."

David Bohm

University of Alberta

Applying Radiation Induced Tissue Damage Models to Cell-Colony Data Analysis and Dose-Volume Constraint Estimation

by

Michael Weldon 

A thesis submitted to the Faculty of Graduate Studies and Research in partial fulfillment of the requirements for the degree of Master of Science

in

Medical Physics

Department of Physics

Edmonton, Alberta

Spring 2006

Your file Votre référence
ISBN: 0-494-13906-4
Our file Notre référence
ISBN: 0-494-13906-4

This work is dedicated to my mother, may she be happy wherever she is.

Abstract

The effects of radiation damage, tumour repopulation, repair and the possibility to extract information about the model parameters describing them are investigated. Published data on cultured cell lines were analyzed by employing a non-Poissonian tumour control probability model. A report in the literature, where *in-vivo* data were analyzed, the employment of the single-hit model of cell kill and cell repopulation produced the best fit. Ignoring the quadratic term of cell damage in the current analysis leads to poor fits. Our data analysis shows the importance of the linear-quadratic mechanism of cell damage for the description of the *in-vitro* cell dynamics.

The possibility of calculating more radiobiologically adequate dose-volume constraints for the needs of the radiation treatment optimization is investigated. Based on the Lyman and the critical volume normal tissue complication probability (NTCP) models, the Monte-Carlo method of reverse NTCP mapping is applied for the calculation of new dose-volume constraint information.

Preface

Chapter 1 outlines the current developments in the radiation biology and the main aspects of the interaction of the radiation with matter. The radiobiological models of cell damage are discussed. Models describing the probability of tumour control after irradiation and the probability of normal tissue complication are described.

Chapter 2 presents the application of the most recent non-Poissonian TCP model to cell megaculture data with the purpose of model parameter values extraction. Our work was published this year (1, see below in List of Publications and Conference Publications) and presented at various conferences (2 and 3, see below in List of Publications and Conference Publications).

In Chapter 3, a reverse mapping approach is applied for the estimation of proper physical dose-volume constraints based on radiobiological considerations for the need of the physical RT optimization. A paper using the work mentioned in this chapter was submitted recently (4, see below in List of Publications and Conference Publications). Material which used the work was presented at two conferences this year, which are listed below (5 and 6, see below in List of Publications and Conference Publications).

Finally, Chapter 4 concludes the findings from the previous two chapters.

List of Publications and Conference Publications

1. P. Stavrev, M. Weldon, B. Warkentin, N. Stavreva, B. G. Fallone. Radiation damage, repopulation and cell recovery analysis of in vitro tumour cell megacolony culture

data using a non-Poissonian cell repopulation TCP model. Physics in Medicine and Biology, Volume 50, Number 13, 7 July 2005, pp. 3053-3061(9)

2. M. Weldon, P. Stavrev, B. Warkentin, N. Stavreva, B. G. Fallone. Radiation Damage, Repopulation and Cell Recovery Analysis of In Vitro Tumour Cell Megacolony Culture Data using a Non-Poissonian Cell Repopulation TCP Model. Alberta Cancer Board Annual Research Meeting, Banff, November 2004
3. P. Stavrev, M. Weldon, B. Warkentin, N. Stavreva, B. G. Fallone. Fitting the Zaider-Minerbo TCP Model to Cell Megacolony Culture Dose Response in Vitro Data. AAPM 2005, American Association of Physicists in Medicine 47th Annual Meeting, July 2005
4. K. Markov, C. Ranger, P Stavrev, N Stavreva, M. Weldon, B. G. Fallone. Reverse Mapping of Normal Tissue Complication Probabilities onto Dose Volume Histogram Space: The problem of randomness of the Dose Volume histogram sampling. Submitted to Medical Physics.
5. C. Ranger, P. Stavrev, M. Weldon, N. Stavreva, R. Scrimger, B. G. Fallone. Reverse NTCP mapping and the problem of physical dose-volume constraint estimation. Cancer Research Across the Spectrum: National Meeting for Trainees, Mont Tremblant, May 2005
6. C. Ranger, P. Stavrev, N. Stavreva , M. Weldon, R. Scrimger, B. G. Fallone. On the dose-volume constraints based on radiobiological considerations. AAPM 2005, American Association of Physicists in Medicine 47th Annual Meeting, July 2005

Acknowledgements

Finishing my Master's degree has been one of the most intensive undertakings of my life thus far. Throughout the past 3 years I have had considerable help, advice and support from many people both within the university and outside of its borders. Without them, this work would not have been completed.

I would first and foremost like to thank Pavel Stavrev for being my supervisor, without his guidance and knowledge (and especially patience) I would not have been able to even start my research. I would like to thank the head of the department and my other supervisor, Gino Fallone, for his motivation and insight in all aspects of my research and graduate endeavors. Brad Warkentin is another person who cannot be forgotten, as he was indispensable in helping me understand radiobiology as well as the research itself. I also must thank Colleen Ranger for her help and assistance in the research. I would like to thank Dave Murray, and though my interaction with him was seldom, he was always a pleasure to talk to (as well as telling me how I had the biology parts of my thesis all wrong).

I must also thank many other people who may not have been quite as involved with the thesis directly, but helped nonetheless. I would like to thank Teo Stanescu for his advice and friendship throughout my time at the CCI. Ryan Rivest and Deluan Tu both survived sharing an office with me, as well as providing me with insight and amusement, which demands gratitude at the very least. I cannot ignore the rest of the graduate students in the department, both long gone and new, so I must thank Tara Monajemi, Steven Thomas, Sandra Vidakovic, and all the rest for attempting to keep me sane and letting me know I'm not the only one going crazy.

There are certain people in the university who have helped make my life considerably easier with their kindness and knowledge. I must thank Lynn Chandler and Sarah Derr, the past and present physics graduate student advisors, for their help when I first arrived in Edmonton and throughout my three years here has been invaluable. I also must thank Jocelyn Martin, Debbi Howorko and Maureen Kostanuick, as they have definitely been a great help with the minute details which seem to plague all graduate students. While I primarily dealt within the medical physics community, I did occasionally need to escape the CCI up to the physics building, where the physics secretaries always were a pleasure to talk to, whether for business or a little lighthearted conversation.

Outside of any department, not involved in my graduate work at all, but without whose help, advice and benevolence I would never have finished, I must thank Asha Sinha, Joanne Yardley and the rest of the staff at the SSDS for helping me discover my faults and turning them into strengths. I must also thank Cristelle Audet and the GSSSG for helping me realize I wasn't alone in the scary world of graduate studies.

Finally, I cannot forget the people in my life who weren't attached to the university at all, but who, because of their support and advice, have helped as no others could have. I first much thank my father, Noel Weldon, his partner, Kathryn Bourdon, and my sister, Jennifer Weldon, for always being there when I needed them, despite the monthly (or weekly) questions of "so when are you going to be done?" I also must thank

Harmanie Shairp and Brian Wynder for their patience and support. Their door (and fridge) were always open if I needed to de-stress. And I cannot forget Christina Cook and Steven Yaskiw, who both helped me stay sane despite rarely seeing me. There are innumerable others who in small ways helped me so much. I cannot possibly mention them all, so I will give a broad thanks to all those who in their own way helped me during this grueling period of my life.

Table of Contents

List of Figures

List of Acronyms

CAIR	Continuous accelerated irradiation
CE	Critical element
CV	Critical volume
DV	Dose volume
DVH	Dose volume histogram
EUD	Equivalent uniform dose
FSU	Functional sub-unit
GMD	Generalized mean dose
IMRT	Intensity modulated radiation therapy
LQ	Linear quadratic
NTCP	Normal tissue complication probability
PDE	Partial differential equation
PTV	Planning treatment volume
RT	Radiation therapy
TCP	Tumour control probability

Chapter 1

Overview of the current developments in radiation induced tissue damage models

1.1 *Introduction*

Radiation therapy can frequently contribute to the cure of a malignancy, or at least to a significant palliative improvement in quality of life. One of the most common means of treatment in a modern medical setting is by means of highly penetrating high-energy photons from a linear accelerator. Several x-ray beams are directed into the patient from various angles and, because of Compton (which predominate at high energies in soft tissue) and photoelectric interactions, each of them is attenuated nearly exponentially as it passes into the body. The resulting high-velocity photons and Compton electrons ionize the tissues they traverse, depositing dose especially in the beams' crossfire region. The production of free radicals and other molecular instabilities leads to damage to DNA and to the tissue microenvironment. That, in turn, is intended to kill the tumour cells.

In this chapter, mathematical models describing cell damage will be introduced. A brief overview of the interaction of the radiation with matter will be given. Mechanisms of tissue damage caused by ionizing particles on a molecular - cellular level are discussed. Finally the models describing the probabilities of tumour control and normal tissue complication will be introduced.

1.2 *Definitions*

Some important definitions of terms used in this thesis are listed below.

TCP - *Tumour control probability*, the probability for zero clonogens surviving after the irradiation.

NTCP - *Normal tissue complication probability*, the probability for complication of certain kind for a given organ at risk after the radiation treatment.

D_{50} - The dose resulting in 50% probability of complication (*NTCP*=0.5).

Integral and differential dose volume histograms are two very important notions widely used in the treatment optimization planning.

Integral dose volume function is defined by the function (V,D) determining the volume V which is irradiated to at least a dose D. Mathematically it is expressed as:

$$V_{\text{int}}(D) = \int_{StructureOfInterest} \Theta(D(\vec{r}) - D) d^3\vec{r} \tag{1.1}$$

where Θ is the Heaviside step function.

Differential dose volume function is *defined by the function (V,D) determining the volume V which is irradiated to a dose D.* Mathematically this is obtained by differentiating the Integral dose volume function leading to:

$$V_{diff}(D) = \int_{StructureOfInterest} \delta(D(\vec{r}) - D) d^3\vec{r}\,, \tag{1.2}$$

where δ denotes the Dirac's δ function.

The corresponding dose-volume histograms are given with:

$$V_i^{\text{int}}(D_i) = \int_{D_i-\Delta}^{D_i+\Delta} dD \int_{StructureOfInterest} \Theta(D(\vec{r}) - D) d^3\vec{r} \tag{1.3}$$

and

$$V_i^{diff}(D_i) = \int_{D_i-\Delta}^{D_i+\Delta} dD \int_{StructureOfInterest} \delta(D(\vec{r}) - D) d^3\vec{r} \,. \tag{1.4}$$

The dose volume histograms are easily calculated from the dose distribution (defining the dose at a certain point ***r*** in the body). They represent a one-dimensional reduction of the three dimensional dose distribution. They are widely used in the radiobiological models developed to determine the probabilities of complication or tumour control. They are very important for intensity-modulated radiation therapy (IMRT) plan optimization using dose-volume constraints.

1.3 *Interaction of Photons with Matter*

1.3.1 Coherent (Classical or Rayleigh) Scattering

When incident photons are scattered by the atoms or molecules as a whole, the interaction takes place without energy transfer. The scattered photons have the same frequency as the incident ones. The cross-section of coherent scattering is greater for lower photon energies, which are not large enough to cause ejection of atomic electrons and ionization of the atoms. After energies of about 100 keV, the cross sections for coherent scattering becomes negligible. This kind of interaction does not cause any changes in the atoms and molecules of the substance, and is thus of no radio-therapeutic interest. At most, coherent scattering contributes to broadening the photon beam slightly.

1.3.2 Compton Scattering

When the incident photons interact with individual quasi-free atomic electrons they transfer part of their energy to the electrons. The electrons being quasi-free, i.e. nearly unbound, acquire kinetic energy as a result of the interaction and leave the atom

(molecule). Thus, the atom (molecule) is ionized. Compton scattering takes place on outer weakly bound electrons. That is why the Compton effect is more essential for light and medium atoms, whose electrons are not very strongly bound and for photon energies in the range 0.1-10 MeV widely used in radiotherapy. Compton scattering is the predominant interaction photons with such energies undergo in water and soft tissue (muscles, connective tissue, fatty tissue). This kind of interaction is of great importance in radiobiology and hence, radiotherapy.

1.3.3 Photoelectric Effect

The photoelectric effect involves the interaction of high energy photons with atoms, resulting in the atoms being ionized and the photons absorbed. Bound electrons are ejected with kinetic energy $E_e=h\nu-\varphi$, where $h\nu$ is the energy of the incoming photon and φ is the binding energy holding the electron to the atom. Free electrons are not subject to this effect. This is a consequence of the laws of energy and momentum conservation, and it has simple classical explanation. Let us imagine a free electron and suppose it absorbs a photon. In a frame where the electron (e-) is initially at rest both laws will give: $\frac{1}{2}m\mathrm{v}_{e^-}^2=\varepsilon$, $p_{e^-}=m\mathrm{v}=p_\gamma=\frac{\varepsilon}{c}$. This would lead to $v=2c$, i.e. to a contradiction with the physical reality (given relativity).

As free electrons do not absorb photons at all, this interaction can only take place on inner atomic electrons that are strongly bound and it is more important for heavy atoms. The photons must have energies somewhat greater than the binding energy of the electrons to be absorbed. The mass attenuation varies approximately with atomic number Z to the power of 3-3.8, for higher and lower Z values respectively. It plays a role in a

limited incident energy interval of the order of the binding energies of the electrons. In body tissue it is insignificant for energies greater than 0.1 MeV.

1.3.4 Electron-Positron Pair Production

Theoretically, at energies no less than twice the rest energy of the electron, 2x0.511 MeV = 1.022 MeV, a photon of energy higher than this can be converted into an e^- - e^+ pair. A single free photon cannot produce an e^- - e^+ pair because the energy and momentum conservation laws cannot be simultaneously fulfilled. The e^- - e^+ pair production can take place only when the photon is within an electromagnetic field (or interacts with another photon). Usually the e^- - e^+ production takes place when the photon is in the strong electric field of atomic nuclei. The larger the atomic number and the greater the photon energy, the greater the probability of an e^- - e^+ pair production. In body tissue this interaction becomes predominant for photon energies greater than 20 MeV, i.e. well above the theoretical threshold. The kinetic energy given to the e^- - e^+ pair (which can be distributed between the positron and electron in any fraction) is then given by $h\nu$ – 1.022 MeV. At such photon energies, the kinetic energy of the produced electrons and positrons is in itself enough to cause inelastic interactions with the medium. Also, photon production by the charged particles (e^- - e^+) can take place either as a result of bremstrahlung or annihilation of the positron with an electron from the medium. The probability of annihilation of a fast positron (1), while passing through matter is quite small, so in most cases a fast positron will first lose all its energy and is then annihilated. As a result of the annihilation process, two photons are produced, each with an energy of at least 0.511 MeV, i.e. these are photons capable of causing Compton interactions. Thus, electron - photon showers may be developed.

1.4 *Interaction of Electrons with Matter*

The energy interval of electrons used in radiotherapy varies from several keV to 20 MeV. These electrons may be considered fast electrons. Fast electrons are electrons whose velocity is much greater than the mean velocity of atomic electrons which is of the order of 10^6 m/s. For comparison the velocity of 10 keV electrons is $6x10^7$ m/s and the velocity of 10 MeV electrons is nearly $3x10^8$ m/s, i.e. they are ultra-relativistic particles.

1.4.1 Elastic Scattering

Fast electrons may interact elastically with the atoms of the medium. As in the case of coherent scattering of photons, these interactions do not cause changes in the state of the atoms or molecules and are of no biological interest. But as far as there is momentum transfer, the electrons get deflected which causes broadening of the electron beam. That is why these events have to be taken into account for the purposes of electron transport description in the medium.

1.4.2 Inelastic Scattering, Collisional Energy Losses

Inelastic scattering includes excitation and ionization of the atoms or molecules of the medium as a result of collisions of the incident electrons with the atomic electrons or atoms and molecules as a whole. These processes are accompanied by energy transfer and thus cause *collisional* energy losses and slowing down of the incident electrons. The inelastic scattering can be examined in the Born approximation like the elastic scattering. The value of the transferred momentum determines the outcome of the interaction (excitation or ionization of the atom).

Low momentum and energy transfers cause excitation of the atoms or molecules. The energy of the excited state can be radiated (in the optical region) or can dissipate in the form of heat. More importantly, it can cause unspecific chemical reactions in the medium.

Large momentum transfer means that the atom receives a large increase in momentum in comparison to the momentum of the atomic electrons. Since free electrons cannot exist in the medium, the low energy secondary electrons are trapped by nearby atoms (molecules) thus causing their ionization, too.

The low energy transfer ionizations together with the excitation events contribute to the so-called continuous collisional energy losses and continuous slowing down of the incident electrons.

In some cases, even though with low probability, the energy exchange can be considerable due to the fact that the interacting particles have equal masses. The secondary (knock-on) electrons can be energetic enough to cause further excitation and ionization of the atoms (molecules) of the medium, i.e. they have a track of their own. Such electrons are called delta rays.

1.4.3 Bremsstrahlung Radiation Losses

When accelerated or decelerated in the electric fields of the atomic electrons and nuclei, the incident electrons like all accelerated charged particles emit photons. This phenomenon is called bremsstrahlung production -a quantum analogue of the synchrotron radiation. It takes place predominantly as a result of interaction with the atomic nucleus as its electric field is stronger by a factor of Z than the field of a single atomic electron.

The intensity of the bremsstrahlung emission is proportional to the particle acceleration, therefore it is inversely proportional to the particle mass. Hence, the bremsstrahlung production is more essential for light particles such as electrons and is quite inessential for heavy particles such as protons and α-particles. The bremsstrahlung photons have a continuous energy spectrum with a sharp bound at the initial energy of the emitting particle.

The bremsstrahlung photons undergo the same interactions as all photons and thus contribute to the development of electron - photon cascades. Thus, the production of bremsstrahlung photons is an additional mechanism of indirect ionization of the medium by the incident electrons.

1.5 *Cellular Radiation Response*

As long as radiation therapy is one of the major modes of the treatment of solid tumours, the prediction of how radiation affects tumours and the human body will be important. Much effort has been directed to the study of the cellular response to radiation, the understanding of which helps us to develop models of tumour control and normal tissue injury by radiation. A discussion of the different models of cellular response to radiation is presented in this section

1.5.1 Single Hit Model

The simplest model for cell death (or survival probability) by radiation is the single hit model. This model assumes that after the cell has been hit with radiation it is dead. A more important assumption is that a cell needs only be 'hit' once by radiation to kill it, a cell can only stay alive if it receives no hits whatsoever. Due to the quantum nature of the processes of high energy particle irradiation, the energy transfer is discrete.

Hence, the dose D could be measured in terms of 'hits per volume'. If v is the volume of the cell or rather the volume of its sensitive structural element, the product vD represents the mean number of hits within the volume v after irradiation with dose D. The four conditions of Poissonian statistics (see Appendix 1) are applicable in this case. Hence, the probability of a cell surviving an irradiation of dose D will be given with:

$$P_{survival} = \frac{\mu^n e^{-\mu}}{n!}, \tag{1.5}$$

where μ is the mean number of hits and n is the number of hits. As mentioned earlier, the mean number of hits is proportional to the dose. Thus, more radiation equates to more possible hits. Since $\mu = vD$, and in order to survive the cell would have to receive zero hits, i.e n=0, the survival probability for a Single Hit model is given as

$$P_{survival} = e^{-\alpha D} = e^{-\frac{D}{D_o}} \tag{1.6}$$

where D_o is the dose required to reduce the survival probability to 0.369 (e^{-1}), and its reciprocal value determines the cells radiosensitivity α. All the relevant radiobiology and radiation physics reside within D_o, which may be a complex function of any number of interesting parameters which may, or may not, be understood.

The same equation could be obtained by assuming that the decrease in the surviving cells dN irradiated to a dose dD is proportional to the number of cells before the irradiation and the dose dD:

$$dN = \alpha N dD, \tag{1.7}$$

hence after the integration

$$N_{survivals}(D) = N_o e^{-\alpha D}, \tag{1.8}$$

where $N_{survivals}$ is the number of cells which are alive after being irradiated with a dose D, and N_o is the initial number of cells alive. The ratio $N_{survivals} / N_o$ gives the surviving fraction of cells *S(D)*, after irradiation with dose D, serving as an estimate of the probability of cell survival.

If we look at a graph of log *P(D)* along the y axis and Dose along the x axis, we would see a linear graph with a slope equivalent to $1/D_o$. However, in cell irradiation experiments the graphs of the surviving fractions *S(D)* are not linear, but in most cases they curve downwards with increasing dose. In the real case, the constant α is not independent of the dose *D*. Integration of Equation (1.8) then leads to a cell survival curve with a shoulder. So while it may be the simplest model for survival probabilities of cells (as it has only one parameter), it is only a very basic approximation.

1.5.2 Linear Quadratic Model of Cell Damage

A more commonly used model for survival probability is the Linear Quadratic model (LQ). It is given with the following equation

$$S(D) = e^{-(\alpha D + \beta D^2)} \tag{1.9}$$

where α and β are radiosensitivity coefficients. This LQ model tends to fit survival curves better than the Single Hit model as it does not give an immediate dose response, but a 'shoulder' at low doses that curves downwards with increasing dose. This tends to represent experimental data more accurately, which tends to have a sigmoid shape (shoulder at first, then decreases monotonically). The LQ model diverges from

experimental data at high doses (due to experimental data tending to be more linear given high dose). The biological explanation of α and β were originally thought to be related to single and double strand breaks. α was thought to represent interactions caused by a single photon, while β represented dual-photon events inflicted on the same local area.

It is now understood that chromosome and chromatid aberrations are responsible for cell death or inactivation. Due to malformed chromosomes (in such patterns as dicentrics or rings), not all of the chromosomes can be properly divided, or even separated, when the cell divides. Given this, it can be thought that single photons that incur these aberrations are represented by α. Likewise, aberrations caused by two photons are represented by β.

There is an alternate explanation, involving lethality of the damage produced by the photons. Given that there are different degrees of damage depending on how the photons interact with the cells (eg: indirect, direct, how much energy is deposited), cells have a varying degree in success on repairing the DNA. Single strand breaks are very easily repaired, as often are smoothly cut double strand breaks. However, mass eliminations of segments of DNA (multiple base pairs) on both sides can produce genetic mutations when reattached. Given multiple double strand breaks as well as the winding, close knit way in which DNA gathers to form chromosomes, chromosomal (and chromatid) aberrations can occur, as mentioned above. Thus the cells' chances of survival are dependent upon the type of damage sustained, whether it is lethal or sub-lethal.

Given lethal damage, a cell will die without any possible ability to recover, but cells receiving sub-lethal damage have the potential to repair themselves. In relation to the LQ model, α would represent lethal damage while β represents sub-lethal damage.

1.6 *Tissue Response to Radiation*

1.6.1 Tumour Control Probability

It is believed that a tumour can repopulate from a single clonogenic cell. The desired outcome of a curative treatment must therefore be the total eradication of all tumour cells. Therefore the probability of zero surviving clonogens after the radiation treatment is sought. This probability is called Tumour Control Probability – TCP. Let *S(D)* be the surviving fraction of clonogens in the tumour, given as $S(D) = \frac{N}{N_o}$, where N_o is the number of initial clonogens and N is the number of clonogens after receiving a dose D. *S(D)* is an estimate of the probability that a cell will survive after receiving a dose D, *1-S(D)* represents the probability that a cell will die given dose D. As there are only two states a cell can be in (alive or dead), we can thus apply the binomial distribution to estimate the probability for observing exactly N survivals out of N_o clonogens

$$P(N) = (S(D))^N (1 - S(D))^{N_o - N} \left(\frac{N_o!}{(N)!(N_o - N)!} \right). \tag{1.10}$$

The probability for zero survivals (N=0) is then given with:

$$TCP = (1 - S(D))^{N_o}. \tag{1.11}$$

This can be converted to the Poisson model given that *S(D)* is small (of course, it is known that the reduction to the Poisson model from the Binomial distribution requires a large N_o value, which is logical because *S(D)* and N_o are inversely proportional). The *TCP* then becomes

$$TCP = (e^{-S(D)})^{N_o} = e^{-N_o S(D)}. \tag{1.12}$$

1.6.2 Fractionation

It has been shown that by splitting the dose into fractions, fewer cells are killed and more total dose is required to maintain the same level of cell death (2). Taking this into consideration, as well as non-trivial cell survival models, it would at first be perceived as foolish to fractionate the dose when the focus is maximizing tumour cell death. Contrary to this, it is common practice for radiotherapy treatments to be fractionated. To understand why one must examine more closely other aspects of cellular responses to radiation.

After being irradiated, cells can repair themselves from sublethal damage. Repopulation also occurs between fractions. However, this happens for normal tissue cells as well as tumour cells. The initial justification for fractionation is from the lower α/β ratios of normal tissue compared to tumours. While early response is similar for both tumours and normal tissue, normal tissue fairs better with each fraction of radiation. It can be seen that despite the greater amount of dose required to achieve the same level of tumour control when implementing fractionation, normal tissue damage could be decreased.

Many biological advancements in understanding the cell replication cycle and how it correlates to the repair of radiation-induced damage (at different points of the cycle) have been made in recent years.

Another reason for using fractionation is allowing hypoxic regions (hypoxic is defined as a deficiency of oxygen in tissue, which causes the cells to be more radioresistant) to be reoxygenated, causing them to be more susceptible to the next fraction. This is due to the clearing of surrounding non-hypoxic cells which were killed off, allowing blood to reach the oxygen deprived cells. On the other hand, even if the sublethal repair rates in the tumour and the normal tissue are equal, the dose delivered to the tumour is considerably higher, hence the damage to the tumour is much greater than to the normal tissue. In addition, the normal tissue is irradiated heterogeneously, there is cellular repair between the irradiations, and there is organ repair on a macro-level. Tissue rescuing units, which are migrating cells from the healthier parts of the organ (receiving very low doses), may help the organ to reestablish some of its damaged functions.

Over the years, the TCP model has been adapted (or completely remade) to take into consideration fractionation, as well as effects that result from repopulation and repair of sublethal damage. The problem of incomplete cell repair has been examined by a number of authors (3-7).

1.6.3 Repopulation: Attempts to Incorporate the Repopulation in the Poissonian Model

Tumour control probability models are usually based on the assumption that the distribution of the surviving cells is subject to the Poisson approximation of the binomial

statistics, and that the cell kill occurs according to either the single hit mechanism or the LQ model of cell damage with complete repair of the cells between any two consecutive fractions (8-19). To incorporate the clonogen repopulation and overcome this lack of completeness in the TCP modeling a number of authors (20-34) have used a modified version of the Poissonian TCP model which incorporates a time-dependent term to account for the process of repopulation.

Cell culture experiments have shown that the increase in the number of cells dN for a time dt due to repopulation is proportional to the number of cells at that moment, N:

$$\frac{dN}{dt} = N\lambda, \tag{1.13}$$

with λ being the proportionality constant or repopulation rate. The solution of this ordinary differential equation is

$$N = N_o \exp(\lambda t). \tag{1.14}$$

Hence if a tumour is left to itself it will repopulate according Equation (1.14). The irradiation to a dose D will reduce the number of cells according to Equation (1.8) (or (1.9) depending on the model of cell damage chosen). In the case when the cellular damage follows the LQ model of cell kill with the assumption of *complete* repair of sublethal damage between fractions, the cell survival probability is

$$S(D) = e^{-(\alpha D + \beta D d) + \lambda T}, \tag{1.15}$$

where d is the dose per fraction. The *TCP* is then given by

$$TCP = e^{-N_o e^{-\alpha D - \beta D d + \lambda T}} \tag{1.16}$$

where D the total dose and T the total treatment time. This is independent of fraction time length, which can be variable.

For non-constant dose per fraction, and incorporating the results for sublethal cell repair, one gets:

$$TCP = e^{N_0 e^{-\alpha D - \beta \sum_{i=1}^{n} d_i^2 - 2\beta \sum_{i=1}^{n-1} \sum_{j=i+1}^{n} d_i d_j e^{\frac{(T_{j-1} - T_{i-1})}{\tau}} + \lambda T}} . \quad (1.17)$$

A more mathematically rigorous approach will be discussed in Section 1.6.4. The derived TCP formula that accounts for repopulation has the following flaws:

- It predicts a *TCP* that always tends to zero for large post treatment times, which is incorrect.
- Only the full treatment time T matters, no account is taken for varying intervals between two consecutive fractions and cell survival probability that changes from fraction to fraction.

1.6.4 Non-Poissonian Models

As early as 1990 the question of the character of the TCP distribution in the presence of repopulation was raised by Tucker *et al* (35):

> *"The results show that although Poisson statistics (based on exact knowledge of all parameters) accurately describes the probability of tumour cure when no proliferation occurs during treatment, it underestimates the cure rate when proliferation does occur"* (35).

The formalism of tumour dynamics that has been developed in the past has been mostly descriptive rather than quantitative. Theoretical modeling of the combined effects of cell kill by radiation and cell dynamics is particularly difficult mainly because the distribution of the surviving tumour cells was found to deviate from the binomial (Poisson)

distribution (35, 36). Nevertheless, theoretical models (37, 38) taking cell repopulation into account have been developed recently. Zaider and Minerbo (37) give a general expression for the probability of zero cells surviving the treatment that is applicable to any fractionation regime and for cell survival probability that may vary from fraction to fraction. The form of the expression makes it also applicable to any treatments protracted in time like brachytherapy, radioactive nuclide applications or any other continuous treatment. In a later work, Zaider *et al* (38) use a more specific expression of the distribution of the number of surviving cells when repopulation is accounted for. This expression, however, is only valid for the special case of equal time intervals between the fractions and for equal cell survival probability for each fraction. These are rather limiting conditions: the former condition is not conventionally fulfilled in clinics; the latter condition is fulfilled only for the simple Single Hit model of cell kill (or the LQ model with complete recovery of the cells between any two consecutive fractions) and when equal doses per fraction are delivered. For this reason, Stavreva *et al* (39) investigated the more generally applicable repopulation model presented in the earlier work of Zaider and Minerbo (37). Based on the Zaider-Minerbo model, Stavreva *et al* (39) derived an explicit expression for the TCP for fractionated external treatments with varying intervals between two consecutive fractions and with cell survival probability that changes from fraction to fraction. This expression allows the incorporation of the more general version of the LQ model of cell damage assuming incomplete recovery of the cells between fractions.

Recently it was demonstrated (39) that the Zaider-Minerbo model is superior to the standard (Poissonian) model description of TCP data from animal experiments.

The Zaider and Minerbo TCP model, which incorporates repopulation without using the Poisson (or binomial) distribution to determine the cell death after irradiation, is based on a birth/death model developed by Kendall in 1948 (40) which can be defined by the following partial differential equation (PDE)

$$\frac{dP_i(t)}{dt} = (i-1)bP_{i-1}(t) - i[b+\delta]P_i(t) + (i+1)\delta P_{i+1}(t) \tag{1.18}$$

where $P_i(t)$ is the probability that at time t there are i clonogens alive, b is the cell birth rate and δ is the cell death rate (41).

By solving the PDE, they created a generalized TCP model,

$$TCP\ (t) = \left[1 - \frac{p(t)e^{(b-d)t}}{\left(1 + bp(t)e^{(b-d)t}\int_0^t \frac{dt'}{p(t')e^{(b-d)t'}}\right)}\right]^n \tag{1.19}$$

where $p(t)$ is the time dependent surviving fraction (not taking into account repopulation, as that is done by $e^{(b-d)t}$), n is the number of initial clonogenic cells and b and d are the radiation independent birth and death rate of the cells respectively. This very adaptable model can use any given surviving fraction, and gives the *TCP* at any point during or after treatment. However, due to the integral, it can be mathematically intensive requiring numerical models. The authors mention that this particular model

> *"predicts that for any dose distribution – not only for a fractionated schedule – the binomial/Poisson versions always underestimate the TCP"* (Zaider and Minerbo, 2000 (37)).

The model does reduce to the binomial model given b=d=0.

Based on the Zaider-Minerbo model, Stavreva *et al* (39) derived an explicit expression for the *TCP* for fractionated external treatments with varying intervals between two consecutive fractions and with cell survival probability that changes from fraction to fraction. This expression allows the incorporation of the more general version of the LQ model of cell damage assuming incomplete recovery of the cells between fractions. By assuming that the dose is given instantaneously (essentially in a small enough time period where no cell repair can happen), and that *S(t)* (time dependent surviving fraction) is time independent between fractions, the resulting model is given by

$$TCP\ (t = T_{i-1}) = \left[1 - \frac{S(T_{i-1})e^{\lambda T_{i-1}}}{\left(1 - S(T_{i-1})e^{\lambda T_{i-1}} \sum_{k=1}^{i-1} S(T_{k-1})\left[e^{-\lambda T_k} - e^{-\lambda T_{k-1}} \right] \right)} \right]^n \qquad (1.20)$$

where T_{i-1} is the time after the *i-1*th fraction, and λ is

> "the net birth rate of cells equal to the difference between their actual birth rate and their death rate" (39).

It uses $S(t) = \exp - \left(\alpha D + \beta \sum_{i=1}^{n} d_i^2 + \beta \sum_{i=1}^{n-1} \sum_{j=i+1}^{n} d_i d_j \exp\left[- \frac{(T_{j-1} - T_{i-1})}{\tau} \right] \right)$ for the surviving fraction, which assumes an exponential rate of recovery for sublethal damage between any two fractions, where τ^{-1} is the probability of cell repair per unit time (see Appendix 3 for the derivation).

The model is not necessarily dependent on time, but instead on the time between each fraction, which is more important given modern treatment methods. Recently it was demonstrated (39) that the Zaider-Minerbo model provides superior results to the standard (Poissonian) model for the description of TCP data from animal experiments.

1.6.5 Organ's or Normal Tissue Response

It was not until the late 70's when some initial attempts were made in the direction of quantifying the response of the normal tissue to radiation (10, 42-45) and some indices such as normal tissue complication probability factor (44) were introduced. During the 80's, the concept of the critical element model of tissue response was dominant ((46-49) and others). In 1982, Wolbarst *et al* (46) introduced a concept similar to that of the damaged volume (47), and in 1988 Withers *et al* (50) introduced a very basic hypothesis which laid the foundation of the mathematical biological modeling of the normal tissue response in the 90's, namely, the notion of functional sub-units (50-52).

1.6.5.1 *Functional Sub-Unit Response Models (Critical Volume and Critical Element Models)*

Based on the hypothesis that the normal tissue is comprised of Functional Sub-Units (FSUs) (50), and that the radiation response of these structural elements is statistically independent, it can be shown that the tissue response to a homogeneous irradiation can be described by one general formula, namely the cumulative binomial distribution (14, 53, 54). The general concept behind this hypothesis is that the probability of causing damage to a normal tissue, NTCP, depends on the probability of damaging a structural element - functional sub-unit, on the functional reserve of the tissue and on the total number of structural elements under irradiation. Depending on whether the irradiation is a whole organ or partial irradiation, this number may be equal to or less than the total number of elements comprising the organ - N. The functional reserve or the critical number of elements M is the number of structural elements that must be damaged

to cause a failure in the structure of interest. The ratio $\mu_{cr}= M/N$ is called relative critical volume. Based on the above discussion and the following assumptions:

- the number of cells in an FSU is constant and cannot vary from FSU to FSU in an organ
- the volume of the organ could be divided into sub-volumes where the dose distribution might be considered homogeneous, with a sufficient number of FSUs in each sub-volume

Jackson *et al* (54) and Niemierko and Goitein (55) have derived the following expression for the tissue response to a heterogeneous irradiation:

$$NTCP = \Phi\left(\frac{\sqrt{N}\left(\sum_i v_i\, p_{FSU}(D_i) - \mu_{cr}\right)}{\sqrt{\sum_i v_i\, p_{FSU}(D_i)\left(1 - p_{FSU}(D_i)\right)}}\right) \tag{1.21}$$

where $\Phi(x) = \frac{1}{\sqrt{2\pi}} \int_{-\infty}^{x} e^{-\frac{t^2}{2}} dt = \frac{1}{2}\left(1 + erf\left(\frac{x}{\sqrt{2}}\right)\right)$, $p_{FSU}(D_i)$ is the probability of damaging an FSU irradiated to a dose D_i and the set (v_i,D_i) represents the differential dose volume histogram. The sum $\sum_i v_i\, p_{FSU}(D_i)$ can be identified as the mean relative damaged volume $\bar{\mu}_d$, the concept for which was first introduced by Wolbarst (integral response organs) (46). The NTCP expressions in the cases of homogeneous partial or whole organ irradiation can be obtained as special cases from Equation (1.21). These expressions can be found in refs. (54, 55).

1.6.5.2 *Probability of FSU Damage*

It is believed that an FSU can repopulate from a single stem cell comprising the FSU. Therefore, an expression similar to the Poissonian *TCP* expression (Equation (1.12)) is commonly used to describe the sub-unit response - $p_{FSU} = e^{-N_{oFSU} p_s}$, where now N_{oFSU} is the total number of stem cells constituting an FSU and p_s is the probability of damaging a cell. The Single Hit model of cell damage is usually assumed sufficient to describe the stem cell response to irradiation - $p_s = e^{-\alpha D}$. The resulting expression for p_{FSU} is:

$$p_{FSU} = e^{-N_{oFSU} e^{-\alpha D}}. \tag{1.22}$$

An expression for p_{FSU} written in terms of the slope γ_{50}^{FSU} and position D_{50}^{FSU} of the FSU response curve is also frequently used:

$$p_{FSU} = \Phi\left(\sqrt{2\pi}\gamma_{50}^{FSU} \ln\frac{D}{D_{50}^{FSU}} \right). \tag{1.23}$$

1.6.6 Population NTCP Models

The TCP and NTCP models described so far are models of individual dose-response. Due to the variation of the different model parameters over the population and the complexity of achieving an individualised treatment, currently the clinically relevant models are the population response models. It is interesting to note that during the 80's most works did not take into account the fact that what researchers were dealing with was actually a population response to radiation. It seems that the models developed in these studies were based on consideration of the individual response of an organ. It was

assumed implicitly that these models could be applied to clinical data, while clinical data is obviously data describing a population response. The first adequate population NTCP model is the Lyman's model (56).

1.6.7 Lyman's NTCP Model

1.6.7.1 *Uniform Irradiation*

Under the assumption that the individual organ response to homogeneous irradiation is infinitely steep ($\gamma_{50} \to \infty$) and therefore can be described by the position of the response curve D_{50} alone and that D_{50} is normally distributed among the population, the probability of complication is given with the cumulative normal distribution:

$$NTCP = \Phi\left(\frac{D - D_{50}}{\sigma_{50}}\right) = \frac{1}{\sqrt{2\pi}} \int_{-\infty}^{\frac{D - D_{50}}{\sigma_{50}}} e^{-\frac{t^2}{2}} dt \,, \tag{1.24}$$

for an organ homogeneously irradiated to dose D. Originally, instead of σ_{50} representing the spread of D_{50} among the population, Lyman used the coefficient of variation m: $\sigma_{50} = mD_{50}$.

1.6.7.2 *Non-Uniform Irradiation*

The case of partial volume (v) uniform irradiation is accounted for by recalculating D_{50} (48, 57) as follows: $D_{50}(v) = D_{50}(WholeOrgan)v^{-n}$, where n is an organ specific unknown parameter. More recently, other authors have proposed a number of ways to account for heterogeneous dose irradiation introducing the dose histogram reduction algorithm scheme (58-61), which is a method for handling non-uniform irradiation of an organ. It involves recursive dose volume reduction, i.e. N-step to (N-1)-

step etc., until there a single-step DVH is left corresponding to a homogeneous irradiation. In the case of heterogeneously irradiated organs the following expression:

$$\left(\sum_{i=1}^{N} v_i \sqrt[n]{D_i} \right)^n , \tag{1.25}$$

was suggested (62, 63), for the uniform equivalent dose. Equation (1.25) also reflects the histogram reduction algorithm proposed by Lyman (59), which, as demonstrated by Niemierko (62), relates closely to the Kutcher and Burman reduction algorithm (60, 61). In fact, Equation (1.25) represents the *generalized mean* (64) *dose* (GMD). By substituting D in Equation (1.24) with the generalized mean dose one obtains

$$NTCP = \Phi \left(\frac{GMD(n, \{v_i, D_i\}) - D_{50}}{\sigma_{D_{50}}} \right) = \Phi \left(\frac{\left(\sum_{i=1}^{N} v_i \sqrt[n]{D_i} \right)^n - D_{50}}{m D_{50}} \right) , \tag{1.26}$$

representing the Lyman's NTCP model in case of heterogeneous irradiations.

1.6.8 Critical Volume NTCP Population Models

In order to obtain a population response model based on an individual model an averaging of the individual responses over the population is required. The individual Critical Volume NTCP model has four parameters (see Equations (1.21) and (1.22)). In general a distribution function is needed to describe the spread of the parameter values over the population. The problem of choosing a distribution function is discussed in details in (54, 55, 65).

Based on the assumption that only the relative critical volume parameter μ_{cr} varies over the population and that it is log-log-normally distributed, the following expression for the population Critical Volume NTCP model is obtained:

$$NTCP_{pop} = \Phi\left(\frac{-\ln\left(-\ln\overline{\mu_d}\right)+\overline{\ln\left(-\ln\mu_{cr}\right)}}{\sigma}\right). \tag{1.27}$$

Here σ is the standard deviation of the log-log-normal distribution of μ_{cr}. Equation (1.27) is one of the most commonly used CV $NTCP_{pop}$ expressions. However, pseudo-numerical experiments (65) have shown that the NTCP model represented by this expression loses its biological meaning, turning into a phenomenological model. Equation (1.27) produces acceptable fits to the data but the best fit parameter values deviate considerably from the parameter values used for the generation of the pseudo-data, i.e. the parameters lose their biological meaning. The explanation of the phenomenon lies in the fact that when deriving Equation (1.27) the population variations of the other 3 individual parameters were ignored.

Assuming that not only the critical volume μ_{cr} but also the radiosensitivity parameter α varies among the population the following CV $NTCP_{pop}$ expression is obtained:

$$NTCP_{pop} = \int_0^{\infty}\Phi\left(\frac{-\ln\left(\ln\overline{\mu_d(\alpha)}\right)+\overline{\ln\left(-\ln\mu_{cr}\right)}}{\sigma}\right)\frac{e^{-\left(\frac{\ln\alpha-\overline{\ln\alpha}}{2\sigma_{\ln\alpha}}\right)^2}}{\sqrt{2\pi}\sigma_{\ln\alpha}\alpha}d\alpha. \tag{1.28}$$

It has been shown (65) that Equation (1.28) when used to fit pseudo-experimental data produces parameter values very close to the true parameter values used for the generation

of the pseudo-data. Therefore, Equation (1.28) can be considered as representing the biologically adequate CV population model. Mathematically, it is more complex than Equation (1.27). However, the power of the contemporary computers makes the numerical integration fast and easy. For calculation purposes, one may consider both Equations (1.27) and (1.28) as identical.

1.7 *References*

1. Dirac PMA. Proc. Camb. Phil. Soc. 1930; 26:361.

2. Elkind MM, Sutton H. Radiation Response of Mammalian Cells Grown in Culture .1. Repair of X-Ray Damage in Surviving Chinese Hamster Cells. Radiation Research 1960;13(4):556-593.

3. Lea DE, Catcheside DG. The mechanism of the induction by radiation of chromosome aberrations in Tradescantia. Journal of Genetics 1942;44(2/3):216-245.

4. Lea DE. Actions of radiations on living cells. 9th printing ed. Cambridge, UK: Cambridge University Press; 1956.

5. Nilsson P, Thames HD, Joiner MC. A generalized formulation of the 'incomplete-repair' model for cell survival and tissue response to fractionated low dose-rate irradiation. Int J Radiat Biol 1990;57(1):127-42.

6. Brenner DJ, Hall EJ. Fractionated high dose rate versus low dose rate regimens for intracavitary brachytherapy of the cervix. I. General considerations based on radiobiology. Br J Radiol 1991;64(758):133-41.

7. Stavreva NA. Radiotherapy Dose Optimization Using Biological Criteria [Doctoral]. Hamilton, New Zealand: University of Waikato; 1997.

8. Fischer JJ. Theoretical considerations in the optimisation of dose distribution in radiation therapy. Br J Radiol 1969;42(504):925-30.

9. Fischer JJ, Moulder JE. The steepness of the dose-response curve in radiation therapy. Theoretical considerations and experimental results. Radiology 1975;117(1):179-84.

10. Brahme A. Dosimetric precision requirements in radiation therapy. In: 18th Use of Computers in Radiation Therapy; 1984; Totonto,Canada; 1984. p. 269-74.

11. Brahme A, Agren AK. Optimal dose distribution for eradication of heterogeneous tumours. Acta Oncol 1987;26(5):377-85.

12. Kallman P, Agren A, Brahme A. Tumour and normal tissue responses to fractionated non-uniform dose delivery. Int J Radiat Biol 1992;62(2):249-62.

13. Goitein M, Niemierko A, P. O. The probability of controlling an inhomogeneously irradiated tumour: A strategem for improving tu-mour control through partial tumour boosting. In: 19th L H Gray Conference: Quantitative Imaging in Oncology.; 1995; Newcastle, UK; 1995. p. 25-39.

14. Niemierko A. Reporting and analyzing dose distributions: a concept of equivalent uniform dose. Med Phys 1997;24(1):103-10.

15. Stavrev PV, Stavreva NA, Round WH. A study of objective functions for organs with parallel and serial architecture. Australas Phys Eng Sci Med 1997;20(1):4-10.

16. Stavreva NA, Stavrev PV, Round WH. Comments on the article 'A model for calculating tumour control probability in radiotherapy including the effects of inhomogeneous distributions of dose and clonogenic cell density'. Phys Med Biol 1995;40(10):1735-8.

17. Tome WA, Fowler JF. Selective boosting of tumor subvolumes. Int J Radiat Oncol Biol Phys 2000;48(2):593-9.

18. Webb S, Nahum AE. A model for calculating tumour control probability in radiotherapy including the effects of inhomogeneous distributions of dose and clonogenic cell density. Phys Med Biol 1993;38(6):653-66.

19. Yaes RJ. Some implications of the Linear Quadratic model for tumor control probability. Int J Radiat Oncol Biol Phys 1988;14(1):147-57.

20. Dale RG. Radiobiological Assessment of Permanent Implants Using Tumor Repopulation Factors in the Linear-Quadratic Model. British Journal of Radiology 1989;62(735):241-244.

21. Dale RG. Time-Dependent Tumor Repopulation Factors in Linear-Quadratic Equations - Implications for Treatment Strategies. Radiotherapy and Oncology 1989;15(4):371-382.

22. Maciejewski B, Withers HR, Taylor JMG, Hliniak A. Dose Fractionation and Regeneration in Radiotherapy for Cancer of the Oral Cavity and Oropharynx - Tumor Dose-Response and Repopulation. International Journal of Radiation Oncology Biology Physics 1989;16(3):831-843.

23. Maciejewski B, Withers HR, Taylor JMG, Hliniak A. Dose Fractionation and Regeneration in Radiotherapy for Cancer of the Oral Cavity and Oropharynx .2. Normal Tissue Responses - Acute and Late Effects. International Journal of Radiation Oncology Biology Physics 1990;18(1):101-111.

24. Taylor JMG, Withers HR, Mendenhall WM. Dose-Time Considerations of Head and Neck Squamous-Cell Carcinomas Treated with Irradiation. Radiotherapy and Oncology 1990;17(2):95-102.

25. Travis EL, Tucker SL. Isoeffect Models and Fractionated Radiation-Therapy. International Journal of Radiation Oncology Biology Physics 1987;13(2):283-287.

26. Tucker SL, Travis EL. Comments on a Time-Dependent Version of the Linear-Quadratic Model. Radiotherapy and Oncology 1990;18(2):155-163.

27. Vandegeijn J. Incorporating the Time Factor into the Linear-Quadratic Model. British Journal of Radiology 1989;62(735):296-298.

28. Vandyk J, Mah K, Keane TJ. Radiation-Induced Lung Damage - Dose-Time-Fractionation Considerations. Radiotherapy and Oncology 1989;14(1):55-69.

29. Wheldon TE, Amin AE. The Linear Quadratic Model. British Journal of Radiology 1988;61(728):700-702.

30. Withers HR, Taylor JMG, Maciejewski B. The Hazard of Accelerated Tumor Clonogen Repopulation During Radiotherapy. Acta Oncologica 1988;27(2):131-146.

31. Roberts SA, Hendry JH. A realistic closed-form radiobiological model of clinical tumor-control data incorporating intertumor heterogeneity. Int J Radiat Oncol Biol Phys 1998;41(3):689-99.

32. Thames HD, Peters LJ, Ang KK. Time-dose considerations for normal-tissue tolerance. Front Radiat Ther Oncol 1989;23:113-30.

33. Thames HD, Bentzen SM, Turesson I, Overgaard M, Van den Bogaert W. Time-dose factors in radiotherapy: a review of the human data. Radiother Oncol 1990;19(3):219-35.

34. Roberts SA, Hendry JH. The delay before onset of accelerated tumour cell repopulation during radiotherapy: a direct maximum-likelihood analysis of a collection of worldwide tumour-control data. Radiother Oncol 1993;29(1):69-74.

35. Tucker SL, Thames HD, Taylor JM. How well is the probability of tumor cure after fractionated irradiation described by Poisson statistics? Radiat Res 1990;124(3):273-82.

36. Tucker SL, Taylor JM. Improved models of tumour cure. Int J Radiat Biol 1996;70(5):539-53.

37. Zaider M, Minerbo GN. Tumour control probability: a formulation applicable to any temporal protocol of dose delivery. Phys Med Biol 2000;45(2):279-93.

38. Zaider M, Zelefsky MJ, Hanin LG, Tsodikov AD, Yakovlev AY, Leibel SA. A survival model for fractionated radiotherapy with an application to prostate cancer. Phys Med Biol 2001;46(10):2745-58.

39. Stavreva N, Stavrev P, Warkentin B, Fallone BG. Investigating the Effect of Cell Repopulation on the Tumor Response to Fractionated External Radiotherapy. Med Phys 2003;30(5):735-42.

40. Kendall DG. On the Generalized Birth-and-Death Process. Annals of Mathematical Statistics 1948;19(1):1-15.

41. Sachs RK, Heidenreich WF, Brenner DJ. Dose timing in tumor radiotherapy: considerations of cell number stochasticity. Math Biosci 1996;138(2):131-46.

42. Goitein M. Review of parameters characterising response of normal connective tissue to radiation. Clin Radiol 1976;27(3):389-404.

43. Herring DF. Methods For Extracting Dose Response Curves From Radiation Therapy Data: A Unified Approach. 6(2):. Int. J. Radiat. Oncol. Biol. Phys. 1980;6(2):225-32.

44. Dritschilo A, Chaffey JT, Bloomer WD, Marck A. The complication probability factor: a method for selection of radiation treatment plans. Br J Radiol 1978;51(605):370-4.

45. Wolbarst AB, Sternick ES, Curran BH, Dritschilo A. Optimized radiotherapy treatment planning using the complication probability factor (CPF). Int J Radiat Oncol Biol Phys 1980;6(6):723-8.

46. Wolbarst AB, Chin LM, Svensson GK. Optimization of radiation therapy: integral-response of a model biological system. Int J Radiat Oncol Biol Phys 1982;8(10):1761-9.

47. Wolbarst AB. Optimization of radiation therapy II: the critical-voxel model. Int J Radiat Oncol Biol Phys 1984;10(5):741-5.

48. Schultheiss TE, Orton CG, Peck RA. Models in radiotherapy: volume effects. Med Phys 1983;10(4):410-5.

49. Yaes RJ, Kalend A. Local stem cell depletion model for radiation myelitis. Int J Radiat Oncol Biol Phys 1988;14(6):1247-59.

50. Withers HR, Taylor JM, Maciejewski B. Treatment volume and tissue tolerance. Int J Radiat Oncol Biol Phys 1988;14(4):751-9.

51. Hendry JH, Thames HD. The tissue-rescuing unit. Br J Radiol 1986;59(702):628-30.

52. Archambeau J, Shymko R. Tissue Population Configuration As A Modifier Of Organ Dose-Response. Int. J. Radiat. Oncol. Biol. Phys. 1988;15(3):727-734.

53. Olsen DR, Kambestad BK, Kristoffersen DT. Calculation of radiation induced complication probabilities for brain, liver and kidney, and the use of a reliability model to estimate critical volume fractions. Br J Radiol 1994;67(804):1218-25.

54. Jackson A, Kutcher GJ, Yorke ED. Probability of radiation-induced complications for normal tissues with parallel architecture subject to non-uniform irradiation. Med Phys 1993;20(3):613-25.

55. Niemierko A, Goitein M. Modeling of normal tissue response to radiation: the critical volume model. Int J Radiat Oncol Biol Phys 1993;25(1):135-45.

56. Lyman JT. Complication probability as assessed from dose-volume histograms. Radiat Res Suppl 1985;8(9):S13-9.

57. Withers HR, Thames HD, Peters LJ. Dose fractionation and volume effects in normal tissues and tumors. Cancer Treat. Symp., 1984;1:75 -83.

58. Lyman JT, Wolbarst AB. Optimization of radiation therapy, III: A method of assessing complication probabilities from dose-volume histograms. Int J Radiat Oncol Biol Phys 1987;13(1):103-9.

59. Lyman JT, Wolbarst AB. Optimization of radiation therapy, IV: A dose-volume histogram reduction algorithm. Int J Radiat Oncol Biol Phys 1989;17(2):433-6.

60. Kutcher GJ, Burman C. Calculation of complication probability factors for non-uniform normal tissue irradiation: the effective volume method. Int J Radiat Oncol Biol Phys 1989;16(6):1623-30.

61. Kutcher GJ, Burman C, Brewster L, Goitein M, Mohan R. Histogram reduction method for calculating complication probabilities for three-dimensional treatment planning evaluations. Int J Radiat Oncol Biol Phys 1991;21(1):137-46.

62. Niemierko A, Goitein M. Calculation of normal tissue complication probability and dose-volume histogram reduction schemes for tissues with a critical element architecture. Radiother Oncol 1991;20(3):166-76.

63. Niemierko A. A generalized concept of Equivalent Uniform Dose, 41th AAPM Annual Meeting, Nashville, 24-29 July,. Med Phys 1999;26(6):1100.

64. Abramowitz M, Stegun IA. Handbook of Mathematical Functions with Formulas, Graphs, and Mathematical Tables,. 9th printing. ed. New York: Dover; 1972.

65. Stavrev P, Stavreva N, Niemierko A, Goitein M. Generalization of a model of tissue response to radiation based on the idea of functional subunits and binomial statistics. Phys Med Biol 2001;46(5):1501-18.

Chapter 2

Radiation damage, repopulation and cell recovery analysis of *in vitro* tumour cell megacolony culture data using a non-Poissonian cell repopulation TCP model

2.1 *Introduction*

In vivo as well as *in vitro* dose response experiments are essential for the testing and ranking of mathematical models designed to evaluate the efficacy of cancer treatment. In this respect, the recent work of Tarnawski *et al.* (1) presenting *in vitro* dose-response-fractionated data from two different cell lines is a welcome contribution. Such experiments are very helpful and present a forum for model testing.

The tumour clonogen probability distribution is an extremely important quantity for whose estimation mechanistic mathematical models are being developed. Tumour control probability (TCP) models are usually based on the assumption that the distribution of the surviving cells is subject to the Poisson approximation of the binomial statistics, and that the cell kill occurs according to either the single hit mechanism or the LQ model of cell damage with complete repair of the cells between any two consecutive fractions (2-13). Clonogen repopulation, resensitization, or cell recovery, with the assumption of incomplete repair between fractions, are routinely not taken into account. To overcome this lack of completeness in the TCP modelling, a number of authors (14-

28) have used a modified version of the Poissonian TCP model which incorporates a time-dependent term to account for the process of repopulation. The Poissonian based TCP model with the artificially added term to account for tumour repopulation in the course of protracted treatments, is given by:

$$TCP = \exp(-\exp(K - \alpha D - \beta D d_{fx} + \lambda t_{OTT})) \quad (2.1)$$

where K is the natural logarithm of the initial number of clonogens ($K = \ln N$), D is the total dose delivered during the treatment, d_{fx} is the dose per fraction, λ is the growth rate, t_{OTT} is the overall treatment time, α and β are the radiosensitivity parameters. This modified Poissonian model with an artificially added term to account for repopulation has been also used by Tarnawski *et al.* (1) for the analysis of their data.

However, during the 1990's, a number of papers (29-34) reported on the non-Poissonian character of the TCP for prolonged treatments of proliferating tumours. As early as 1990, Tucker, Thames and Taylor (29) suggested that the distribution of the surviving clonogens must be expected to deviate from the binomial distribution because of cell proliferation that occurs between fractions of irradiation. Although it was recently shown by Hanin *et al* (32) that the limiting distribution of the number of surviving clonogens is in fact Poissonian, it has the following flaws:

- It predicts a TCP that always tends to zero for large post treatment times, which is incorrect (35).
- It only considers the full treatment time T. No account is taken for varying intervals between two consecutive fractions and cell survival probability that changes from fraction to fraction.

In 2000, Zaider and Minerbo (33) constructed an exact expression that describes the distribution of proliferating clonogens having survived a protracted treatment, on whose basis a TCP formula was derived. Based on the Zaider-Minerbo TCP model, Stavreva *et al* (35) derived a TCP expression specific for external fractionated treatments and applicable for the general case of variable probability of cell kill per dose fraction.

Since tumour proliferation may have an appreciable impact on the treatment outcome we consider it important that the Zaider-Minerbo TCP model be applied for the analyses of fractionated treatments rather than the Poissonian or even the modified Poissonian model. In the work presented in this thesis, we analyzed the Tarnawski *et al.* (1) experimental *in vitro* data by using the TCP expression derived by Stavreva *et al* (35).

2.2 *Method and Materials*

2.2.1 Zaider-Minerbo TCP Model

We obtained, from the Zaider-Minerbo TCP model (33), the following TCP expression valid for the case of external radiation with different time intervals between any two consecutive fractions and varying cell survival probability per dose delivery (35):

$$TCP(t = T_{n-1}) = \left[1 - \frac{p_s(T_{n-1})e^{\lambda T_{n-1}}}{\left(1 - p_s(T_{n-1})e^{\lambda T_{n-1}} \sum_{k=1}^{n-1} p_s^{-1}(T_{k-1}) \left[e^{-\lambda T_k} - e^{-\lambda T_{k-1}} \right] \right)} \right]^N \tag{2.2}$$

where N is the initial number of clonogens, λ is the cell repopulation rate, T_{n-1} is the overall treatment time, T_{k-1} is the time until after the k^{th} fraction, and $p_s\left(T_{k-1}\right)$ is the

cell survival probability after the k^{th} fraction of dose delivery. When the spontaneous death rate is not negligible in comparison to the birth rate λ should be considered the net birth rate of cells equal to the difference between their actual birth rate and their death rate. According to the LQ model of cell kill with partial repair of sublethal damage (35, 36), the cell survival probability $p_s\left(T_{k-1}\right)$ is

$$p_s\left(T_{k-1}\right) = e^{-\alpha\sum_{i=1}^{k} d_i} e^{-\beta\sum_{i=1}^{k} d_i^2 - 2\beta\sum_{i=1}^{k-1}\sum_{j=i+1}^{k} d_i d_j e^{-\frac{(T_{j-1}-T_{i-1})}{\tau}}}, \qquad (2.3)$$

where α and β are the cell radiosensitivity characteristics, τ^{-1} is the probability of sublethal damage repair per unit time, d_i is the dose per fraction 'i'. A value of $\tau^{-1} = 0$ corresponds to the case of no recovery of the cells, a value of $\tau^{-1} \neq 0$ corresponds to the case of partial recovery of the cells and a value of $\tau^{-1} \to \infty$ corresponds to the case of complete recovery of the cells between any two consecutive fractions (see Appendix 3).

2.2.2 Data

The Zaider/Minerbo model is sufficienlty flexible that it can be used on either *in vivo* (such as data from Fischer *et al* (3)) or *in vitro* data. This is interesting as it is uncommon to see in vitro data produced that allows *TCP* to be calculated, as the work has to be quite extensive to produce the proper fractionated schemes. Normally only surviving fraction vs dose plots are produced from in vitro data. Given the alterations by Stavreva *et al* (35), any fractionated treatment can be easily fitted. Unfortunately, parameters including the number of cells, radiosensitivity and repopulation coefficients,

can not be compared between *in vivo* and *in vitro* due to very different environmental influences.

The data that was used in Stavreva *et al* (35) was obtained from experiments presented by Fischer *et al* (3). It their experiments, they induced localized, non-metastasized tumours to genetically similar rats (the rats were from the same strain). When the tumours reached ~7.5mm (~10^7-10^8 cells per tumour), they irradiated homogeneously under different fractionating schemes (always on a Monday/Wednesday/Friday schedule), after which there would be a follow up period of 120 days. The animal was deemed cured if there was no recurrence of any tumours. Comparatively, instead of *in vivo* data, Tarnawski *et al* (1) did experiments *in vitro*. Two cell types - AT478 (murine squamous cell carcinoma of the cervix) and A549 (human lung adenocarcinoma cells) were used in the experiments performed by Tarnawski *et al* (1). The cells were grown in DMEM and DMEM/F12 growth medium respectively, supplemented with fetal bovine serum and antibiotics. The cells were then resuspended in growth medium, the number of cells per volume approximating $1x10^6$/mL. On the bottom of flasks, 9 carefully spaced drops of cell suspension were arranged, containing ~50μL (about $5x10^4$ cells). These were then incubated to enable attachment of the cells and then covered in growth medium. After being incubated again (for ~ one week), the cells developed into megacolonies of about 1 cm in diameter. The statistic per experimental dose response point (the total number of cases per point) was presumed to be 9, because each flask irradiated to a given dose contained 9 megacolonies of cells prior to the treatment. The statistic per point is an important quantity for the estimation of the goodness of fit.

The colonies were homogeneously irradiated for three different fractionated schemes - acute treatment (single dose), consecutive daily treatment (Continuous Accelerated Irradiation - CAIR) and conventional treatment. The flasks that received the acute treatment were irradiated with single doses of gamma rays ranging from 8-30 Gy. They were then incubated for 1-4 months to determine if regrowth occurred. Flasks that were used for the CAIR fractionation scheme received 2 Gy of radiation every day (including weekends) until the total dose was delivered. For conventional treatment, flasks received 2 Gy of radiation every weekday (not on weekends), which mimics the current method of fractionation used in radiotherapy. This continued until the total dose was administered. For both CAIR and conventional fractionation schemes, doses ranging from 16-80 Gy were used. Also, both schemes were incubated for 1-4 months after the final fraction was delivered to determine if regrowth occurred. In all treatment schemes, megacolonies were considered dead if no regrowth was observed after 3 months. Radiation was delivered using a 60-Co gamma source, at a dose rate of 0.82 Gy/min.

2.2.3 Data Analysis

The TCP expression given by Equations (2.2) and (2.3) was used to analyze the data published in the Tarnawski *et al* (1) paper using the maximum likelihood methodology of fitting models to data (28, 37-39) and a Monte Carlo based optimization technique for searching for functional minima (39). Following Press (37) and Collet (40), the goodness of fit is calculated from the deviance $Dev = -2\left(\ln L_{\max} - \ln L_{full}\right)$, where L_{full} and L_{max} represent the log-likelihood of the full model (see Collet (40)) and the maximum log-likelihood of the best fit of the model to the data, respectively. The deviance has an

asymptotic χ^2 distribution. The p-value is calculated using, $p = \int_{Dev}^{\infty} \chi_\nu^2(x)dx$, where χ_ν^2 is the chi-square function for ν degrees of freedom, and ν is equal to the number of data points minus the number of free fitting parameters. Conventionally, fits that yield a p-value of less than 5% are considered statistically unacceptable.

The original code used in Stavreva *et al* (35) was used to fit the Tarnawski *et al* (1) data; however, it had to be altered slightly in order to accommodate the differences between the two data sets. The code originally used constant maximum doses allowing for different fractionation schemes dictated in Fischer *et al* (3), but had to be altered to allow for the alternate fractionating schemes given in Tarnawski *et al* (1). In Stavreva *et al*, the number of fractions was kept constant for a given dose-response curve. However, the Tarnawski *et al* data had a constant dose per fraction for all cell lines. This detail actually simplified the code after it was modified for the Tarnawski *et al* data. the modifications that were made simplified the code. See Appendix 2 for the MATLAB code.

2.3 *Results*

We first investigated a simpler version of the TCP model that corresponds to the case of complete cell recovery between any two consecutive fractions, i.e. the case of $\tau^{-1} \to \infty$ ($\tau = 0$, i.e. p_s is no longer time dependent and becomes $p_s(T_{k-1}) = e^{-\alpha\sum_{i=1}^{k} d_i} e^{-\beta\sum_{i=1}^{k} d_i^2}$), thus reducing the number of model parameters to be fitted by one. The resulting fits for megacolony cultures, AT478 and A549, are shown in Figs. 2.1 (a) and 2.1 (b), respectively.

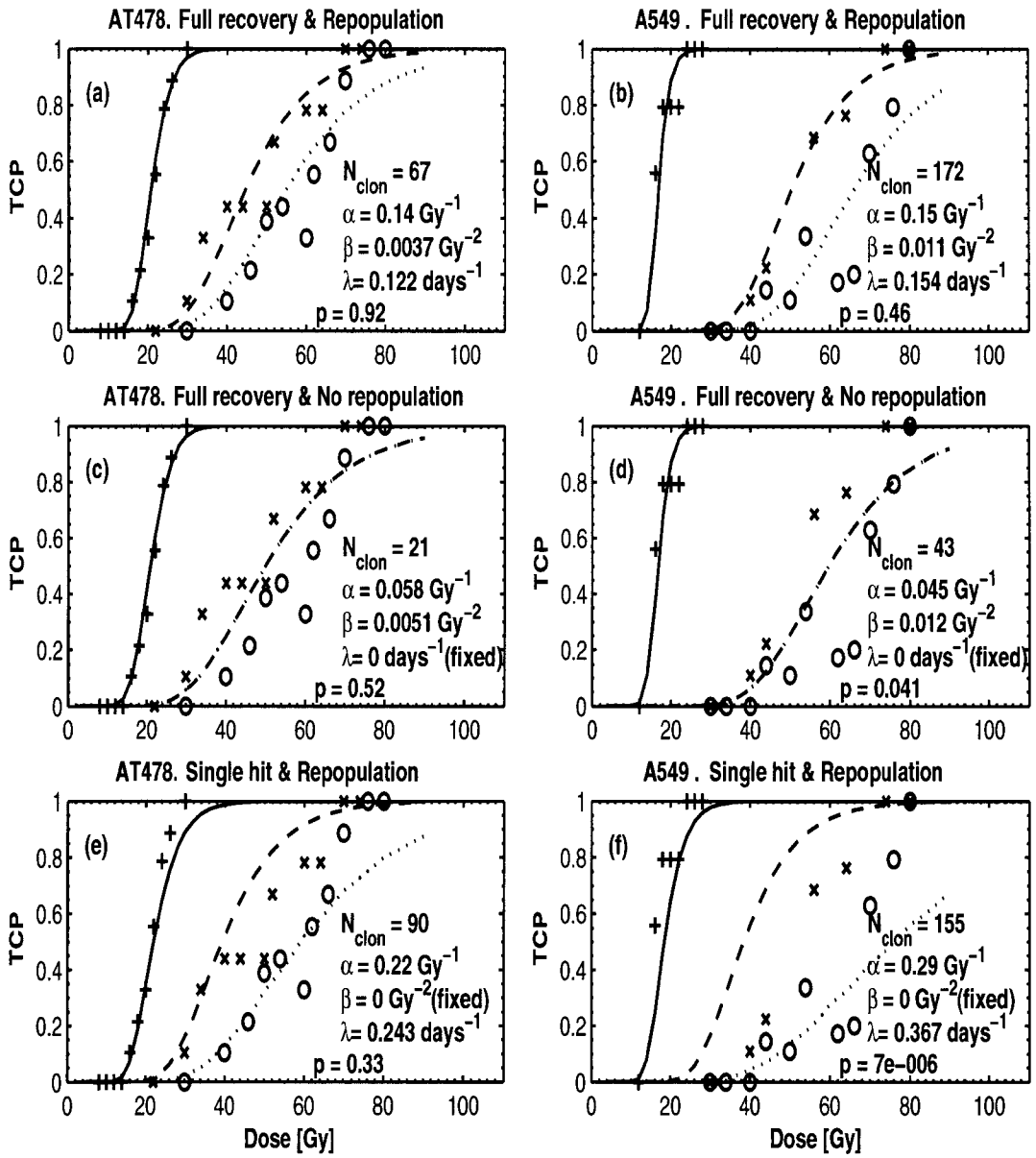

Figure 2.1 Fits of **(a)** and **(b)** a TCP model assuming full recovery of the cells between fractions and repopulation; **(c)** and **(d)** a TCP model assuming full recovery of the cells between fractions and no repopulation; **(e)** and **(f)** a TCP model assuming single hit mechanics of cell damage and repopulation to the Tarnawski et al megacolony culture data. The solid lines and + represent the corresponding model single dose response, the dashed lines and x represent the CAIR dose response, and the dotted lines and o are the conventional treatment dose response.

Two other cases were investigated by setting to zero some of the other model parameters besides τ. Firstly, a case was investigated in which it was assumed that no cell repopulation ($\lambda = 0$, i.e. *TCP* simplifies to $(1 - p_s)^N$) and complete cell recovery between any two consecutive fractions ($\tau = 0$) were taking place. This was done with the purpose of checking the impact of cell repopulation via comparing this case with the case of active cell repopulation ($\lambda \neq 0$) and complete cell recovery ($\tau = 0$). The resulting fits for this case are shown in Figs. 2.1 (c) and 2.1 (d) for the two cultures, AT478 and A549, correspondingly.

Another case was investigated in which the β mechanism of cell kill was assumed inactive ($\beta = 0$, i.e. $p_s\left(T_{k-1}\right) = e^{-\alpha\sum_{i=1}^{k} d_i}$), i.e. it was assumed that the cell kill took place solely via the single hit mechanism of cell damage. Biologically with $\beta = 0$, cell recovery has no meaning as a cell is killed with a single hit (no sublethal damage). At the same time it was assumed that cell repopulation was taking place ($\lambda \neq 0$). This case was studied to check the role of the β mechanism of cell kill. The resulting fits for megacolony cultures, AT478 and A549, are shown in Figs. 2.1 (e) and 2.1 (f), respectively.

We then included the partial recovery in the model by making τ a free parameter of the fit. In this partial recovery mode we investigated two cases. When it was assumed that cell repopulation was present during the treatment ($\lambda \neq 0$), the fits shown in Figs. 2.2 (a) (AT478) and 2.2 (b) (A549) were obtained. In the second case, no cell repopulation

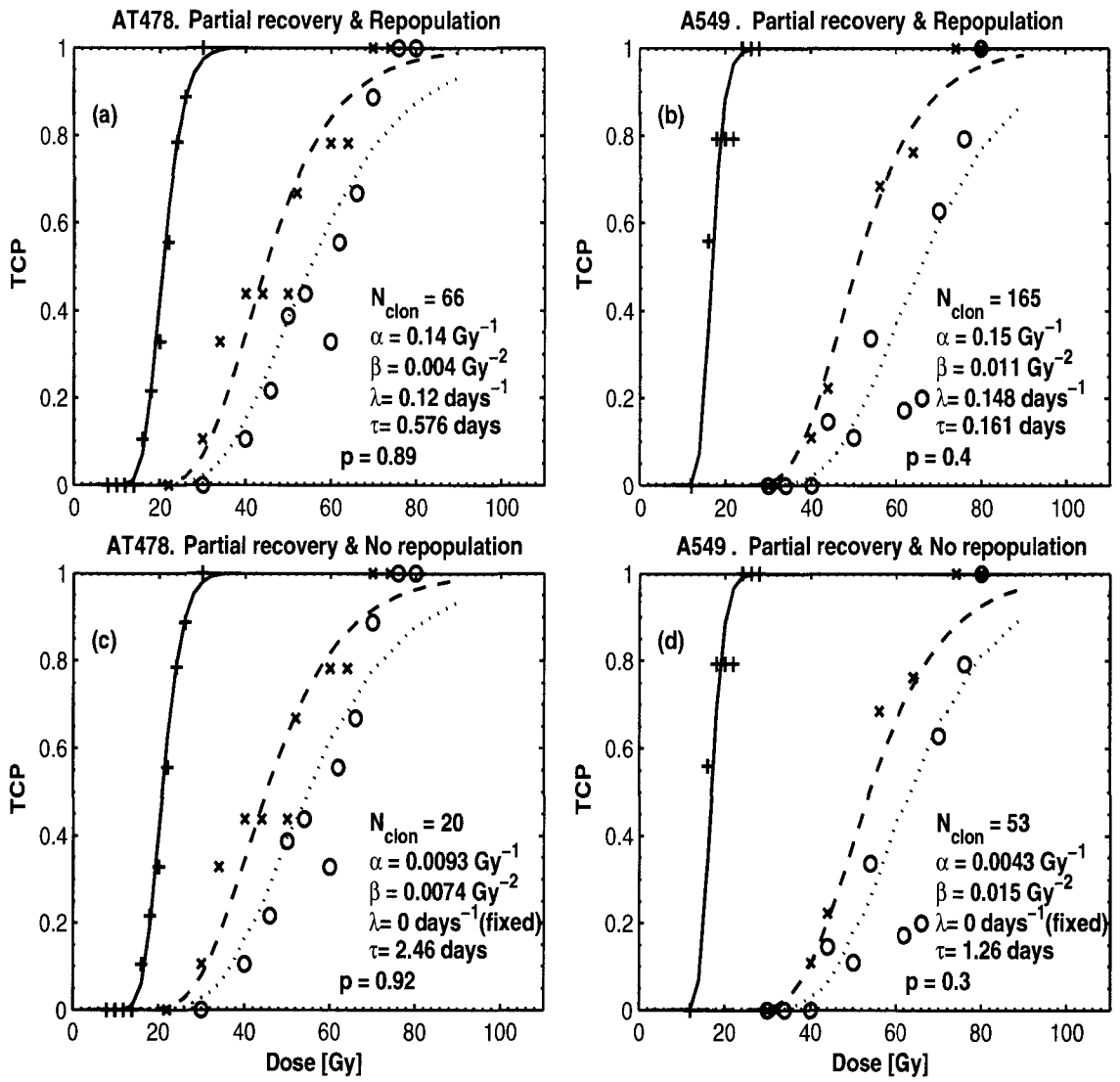

Figure 2.2 Fits of **(a)** and **(b)** a TCP model assuming partial recovery of the cells between fractions and repopulation; **(c)** and **(d)** a TCP model assuming partial recovery of the cells between fractions and no repopulation to the Tarnawski et al megacolony culture data. The solid lines and + represent the corresponding model single dose response, the dashed lines and x represent the CAIR dose response, and the dotted lines and o are the conventional treatment dose response.

was assumed through setting λ to zero ($\lambda = 0$). The corresponding fits for megacolony cultures, AT478 and A549 are shown in Figs. 2.2 (c) and 2.2 (d).

2.4 *Discussion and Conclusions*

The first conclusion that can be made when comparing the p-values of all the fits is that the version of the Zaider-Minerbo model that assumes full recovery of the cells between any two consecutive fractions accompanied by cell repopulation best fits the data from both cellular cultures. This can be seen by comparing the fit in Fig. 2.1 (a) to the fits in Figs. 2.1 (c) and 2.1 (e), and likewise, by comparing Fig. 2.1 (b) to Fig. 2.1 (d) and 2.1 (f). Because of the low best fit values of τ, 0.58 days for AT478 and 0.16 days for A549, the case of partial recovery of the cells accompanied by cell repopulation (Figs. 2.2 (a) and 2.2 (b)) actually reduces to the case of full recovery and repopulation for both cellular cultures. The best fit values of τ for both cell cultures are very close to zero, indicating that full recovery of the cells occurs between any two consecutive fractions. Also, the best fit values of the rest of the parameters are virtually the same as those of the corresponding parameters in the case of full recovery and repopulation. The somewhat lower p-values in the latter case are due to the number of the fitted parameters is higher.

Figures 2.1 (c) and 2.1 (d) illustrate that the model that assumes full recovery of the cells and no cell repopulation does not describe the data well. This model does not distinguish between the two applied fractionation schemes, the CAIR and the conventional one, predicting the same outcome in both cases. Indeed, according to this model, the sublethal damage effectively occurs immediately. Biologically, however, it is more realistic to view the recovery time as being very small with respect to the time between fractions. This, in combination with the assumed inactive cell repopulation,

makes the treatment outcome independent of the time interval between the fractions, and therefore alike for the two fractionation schemes. The data, however, show that the outcome is different for the two fractionation schemes. The conclusion that this model does not fit the data well is confirmed by the very low p-value of the fit in the case of cell type A549. A p-value of 0.04 makes the fit statistically unacceptable. In the case of cell type AT478, a quite high p-value is achieved despite the obviously different outcome for the two fractionation schemes as shown by the data points. This can be explained by the rather low statistics per point, and the fact that the points corresponding to the CAIR (crosses) and to the conventional fractionation scheme (circles) do not lie very far apart. We did not attempt to use a model that assumes single-hit mechanism without repopulation, as this would not distinguish between any fractionation schemes including acute treatments.

Judging by the p-values which allow easy ranking of the models, the version of the Zaider-Minerbo model that assumes single hit mechanism of cell kill accompanied by repopulation offers the worst fit to the data from both cellular cultures. It is interesting to compare this result with a result reported by Stavreva *et al* (35), where the Zaider-Minerbo model was fit to experimental animal data. Stavreva *et al* (35) concluded that the version of the model which best fits the data was the one assuming the single hit mechanism of cell kill and cell repopulation. However, in a later work by Stavreva *et al* (41), a version of the model was developed that accounted for possible reoxygenation of the tumour occurring between treatment fractions. Under that scenario, the model that best fits the data turned to be the one that assumed full recovery of the cells between the fractions accompanied by reoxygenation and cell repopulation. Therefore, it could be

concluded that the consistency and the applicability of the LQ model are preserved in *in vivo,* as well as *in vitro* processes. Also, it should be pointed out that there is no discrepancy between the results reported in (35) and the newly developed approach accounting for initial tumour resensitization in (41). In the first case, where one desires to describe only treatments with high number of fractions, the complexity of the LQ model becomes unnecessary, the effects are so small that the more complex model developed in (41) shrinks from a seven-parametric one to a three-parametric one. In general, one can say that the difference in the manifestation of the β mechanism may be attributed to differences between the *in vivo* and *in vitro* conditions of irradiation and additionally, to differences in the fractionation regimes.

A somewhat unexpected result is the extremely good fit achieved by the model with the assumption of the partial recovery of the cells between fractions without cell repopulation (Figs. 2.2 (c) and 2.2 (d)). Based on the p-values of the fits, this fit for cell type A549 is third to the fit of the model that assumes full cell recovery and cell repopulation (compare Fig. 2.2 (d) with Fig. 2.1 (b)). For cell type AT478, the fit that assumes partial recovery of the cells between fractions and no cell repopulation is as good as the fit of the model that assumes full cell recovery and cell repopulation (compare Fig. 2.2 (c) with Fig. 2.1 (a)). Therefore, based on statistical criteria only, the two models are virtually equally acceptable. However, the good fits are achieved at the expense of rather unusual best fit values of α and β for both cell types. The best fit value of α is quite low, i.e. $\alpha = 0.0093\ Gy^{-1}$ for AT478 and $\alpha = 0.0043\ Gy^{-1}$ for A549 (the usual range of values for α from many experiments is $\alpha \in [0.1 \div 0.3] Gy^{-1}$), while the best fit value of β is comparable to the value of α (it is accepted, that for most tumour

lines, the value of β is about an order of magnitude lower than the value of α). The role of the β mechanism is artificially increased in this model through the high value of β accompanied by a rather slow repair ($\tau = 2.46\ days^{-1}$), which compensates for the inactive repopulation and makes the three fractionation regimes distinguishable. Therefore, we would like to recommend the design of experiments using multiple fractionation regimes to produce diverse data which would potentially allow the acceptance or rejection of models based on statistical criteria rather than on *a priori* knowledge of model parameter values. In particular, as opposed to fractionation schemes evident from Tarnawski *et al* (1) or Fischer *et al* (3), which show fractionation schemes revolving around 1-3 day delays between fractions, experiments should be created giving consideration to actual biological repair cycles. Given that cells have been found to repair themselves over a matter of hours, perhaps delays between fractions of 12, 6 and 3 hours would provide a more accurate basis for understanding mathematically the repair mechanism, as well as potentially provide alternative fractionation schemes clinically.

2.5 *References*

1. Tarnawski R, Widel M, Skladowski K. Tumor cell repopulation during conventional and accelerated radiotherapy in the in vitro megacolony culture. International Journal of Radiation Oncology Biology Physics 2003;55(4):1074-1081.

2. Fischer JJ. Theoretical considerations in the optimisation of dose distribution in radiation therapy. Br J Radiol 1969;42(504):925-30.

3. Fischer JJ, Moulder JE. The steepness of the dose-response curve in radiation therapy. Theoretical considerations and experimental results. Radiology 1975;117(1):179-84.

4. Brahme A. Dosimetric precision requirements in radiation therapy. In: 18th Use of Computers in Radiation Therapy; 1984; Totonto,Canada; 1984. p. 269-74.

5. Brahme A, Agren AK. Optimal dose distribution for eradication of heterogeneous tumours. Acta Oncol 1987;26(5):377-85.

6. Kallman P, Agren A, Brahme A. Tumour and normal tissue responses to fractionated non-uniform dose delivery. Int J Radiat Biol 1992;62(2):249-62.

7. Goitein M, Niemierko A, P. O. The probability of controlling an inhomogeneously irradiated tumour: A strategem for improving tu-mour control through partial tumour boosting. In: 19th L H Gray Conference: Quantitative Imaging in Oncology.; 1995; Newcastle, UK; 1995. p. 25-39.

8. Niemierko A. Reporting and analyzing dose distributions: a concept of equivalent uniform dose. Med Phys 1997;24(1):103-10.

9. Stavrev PV, Stavreva NA, Round WH. A study of objective functions for organs with parallel and serial architecture. Australas Phys Eng Sci Med 1997;20(1):4-10.

10. Stavreva NA, Stavrev PV, Round WH. Comments on the article 'A model for calculating tumour control probability in radiotherapy including the effects of inhomogeneous distributions of dose and clonogenic cell density'. Phys Med Biol 1995;40(10):1735-8.

11. Tome WA, Fowler JF. Selective boosting of tumor subvolumes. Int J Radiat Oncol Biol Phys 2000;48(2):593-9.

12. Webb S, Nahum AE. A model for calculating tumour control probability in radiotherapy including the effects of inhomogeneous distributions of dose and clonogenic cell density. Phys Med Biol 1993;38(6):653-66.

13. Yaes RJ. Some implications of the Linear Quadratic model for tumor control probability. Int J Radiat Oncol Biol Phys 1988;14(1):147-57.

14. Dale RG. Radiobiological Assessment of Permanent Implants Using Tumor Repopulation Factors in the Linear-Quadratic Model. British Journal of Radiology 1989;62(735):241-244.

15. Dale RG. Time-Dependent Tumor Repopulation Factors in Linear-Quadratic Equations - Implications for Treatment Strategies. Radiotherapy and Oncology 1989;15(4):371-382.

16. Maciejewski B, Withers HR, Taylor JMG, Hliniak A. Dose Fractionation and Regeneration in Radiotherapy for Cancer of the Oral Cavity and Oropharynx - Tumor Dose-Response and Repopulation. International Journal of Radiation Oncology Biology Physics 1989;16(3):831-843.

17. Maciejewski B, Withers HR, Taylor JMG, Hliniak A. Dose Fractionation and Regeneration in Radiotherapy for Cancer of the Oral Cavity and Oropharynx .2. Normal Tissue Responses - Acute and Late Effects. International Journal of Radiation Oncology Biology Physics 1990;18(1):101-111.

18. Taylor JMG, Withers HR, Mendenhall WM. Dose-Time Considerations of Head and Neck Squamous-Cell Carcinomas Treated with Irradiation. Radiotherapy and Oncology 1990;17(2):95-102.

19. Travis EL, Tucker SL. Isoeffect Models and Fractionated Radiation-Therapy. International Journal of Radiation Oncology Biology Physics 1987;13(2):283-287.

20. Tucker SL, Travis EL. Comments on a Time-Dependent Version of the Linear-Quadratic Model. Radiotherapy and Oncology 1990;18(2):155-163.

21. Vandegeijn J. Incorporating the Time Factor into the Linear-Quadratic Model. British Journal of Radiology 1989;62(735):296-298.

22. Vandyk J, Mah K, Keane TJ. Radiation-Induced Lung Damage - Dose-Time-Fractionation Considerations. Radiotherapy and Oncology 1989;14(1):55-69.

23. Wheldon TE, Amin AE. The Linear Quadratic Model. British Journal of Radiology 1988;61(728):700-702.

24. Withers HR, Taylor JMG, Maciejewski B. The Hazard of Accelerated Tumor Clonogen Repopulation During Radiotherapy. Acta Oncologica 1988;27(2):131-146.

25. Roberts SA, Hendry JH. A realistic closed-form radiobiological model of clinical tumor-control data incorporating intertumor heterogeneity. Int J Radiat Oncol Biol Phys 1998;41(3):689-99.

26. Thames HD, Peters LJ, Ang KK. Time-dose considerations for normal-tissue tolerance. Front Radiat Ther Oncol 1989;23:113-30.

27. Thames HD, Bentzen SM, Turesson I, Overgaard M, Van den Bogaert W. Time-dose factors in radiotherapy: a review of the human data. Radiother Oncol 1990;19(3):219-35.

28. Roberts SA, Hendry JH. The delay before onset of accelerated tumour cell repopulation during radiotherapy: a direct maximum-likelihood analysis of a collection of worldwide tumour-control data. Radiother Oncol 1993;29(1):69-74.

29. Tucker SL, Thames HD, Taylor JM. How well is the probability of tumor cure after fractionated irradiation described by Poisson statistics? Radiat Res 1990;124(3):273-82.

30. Yakovlev AY. Comments on the Distribution of Clonogens in Irradiated Tumors. Radiation Research 1993;134(1):117-120.

31. Kendal WS. A closed-form description of tumour control with fractionated radiotherapy and repopulation. International Journal of Radiation Biology 1998;73(2):207-210.

32. Hanin LG, Zaider M, Yakovlev AY. Distribution of the number of clonogens surviving fractionated radiotherapy: a long-standing problem revisited. Int J Radiat Biol 2001;77(2):205-13.

33. Zaider M, Minerbo GN. Tumour control probability: a formulation applicable to any temporal protocol of dose delivery. Phys Med Biol 2000;45(2):279-93.

34. Zaider M, Zelefsky MJ, Hanin LG, Tsodikov AD, Yakovlev AY, Leibel SA. A survival model for fractionated radiotherapy with an application to prostate cancer. Phys Med Biol 2001;46(10):2745-58.

35. Stavreva N, Stavrev P, Warkentin B, Fallone BG. Investigating the Effect of Cell Repopulation on the Tumor Response to Fractionated External Radiotherapy. Med Phys 2003;30(5):735-42.

36. Stavreva NA. Radiotherapy Dose Optimization Using Biological Criteria [Doctoral]. Hamilton, New Zealand: University of Waikato; 1997.

37. Press WH, Flannery BP, Teukolsky SA, *al. e.* Numerical Recipes. 9th printing. ed. Cambridge: Cambridge University Press; 1986.

38. Jackson A, Ten Haken RK, Robertson JM, Kessler ML, Kutcher GJ, Lawrence TS. Analysis of clinical complication data for radiation hepatitis using a parallel architecture model. Int J Radiat Oncol Biol Phys 1995;31(4):883-91.

39. Stavrev P, Stavreva N, Niemierko A, Goitein M. The Application of Biological Models to Clinical Data. *Phys Medica* 2001;XVII(2):71-82.

40. Collet D. Modelling binary data: Chapman & Hall; 1991.

41. Stavreva N, Warkentin B, Stavrev P, Fallone BG. Investigating the Effect of Clonogen Resensitization on the Tumor Response to Fractionated External Radiotherapy. Med Phys 2005;in print.

Chapter 3

On Dose-Volume constraints based on radiobiological considerations. An algorithm of Dose Volume histogram random sampling

3.1 *Introduction*

In clinical practice several dose-volume constraints are usually simultaneously specified in the process of radiation treatment (RT) optimization. Currently these constraints relate to partial organ irradiations (1), equivalent to single step dose-volume histograms (DVH), resulting in a normal tissue complication probability (*NTCP*), of 5%. Combining two or more such dose volume constraints is unadvisable, since they will no longer result in the expected 5% *NTCP*. Although the RT optimization based on radiobiological indices is still in its infancy, a reverse NTCP mapping method (2) was proposed, based on radiobiological indices, for the proper estimation of the physical dose-volume constraints for the needs of the inverse RT planning. In this chapter, based on the Lyman and the Critical Volume NTCP models, the Monte Carlo method of reverse NTCP mapping is applied to calculate proper dose volume constraints for organs for which parameter value information is available (3, 4). Based on clinical information about the maximal dose-range to which an organ may be irradiated during the RT, 10^6 DVHs are simulated. From this set of DVHs, the DVHs producing an $NTCP \in \{5 \pm 0.5\%\}$ are selected. An average DVH is produced from the selected DVHs. Its values are proposed to serve as dose-volume constraints in the process of inverse

treatment planning. Currently there is only one main compendium of dose-volume NTCP data given (1). However, it is shown that indeed a DVH passing through a combination of constraints as specified in Emami *et al.* (1) is well outside the range of the DVHs producing $NTCP \in \{5 \pm 0.5\%\}$. The proposed method helps in creating new dose-volume constraint information.

3.2 *NTCP Models used for Reverse Mapping*

The two models used to calculate *NTCP* in this project are the Lyman model and the CV model (see Sections 1.6.7 and 1.6.8, respectively). The population version of the CV model in particular is used, as the Emami *et al* DV constraints are for the average population.

3.3 Method

In this section, a general overview of the method of reverse mapping is presented. The goal of this project is to create the software for random integral DVH sampling and to apply it for the estimation of dose constraint points for values of *NTCP*=5+/-0.5%.

The problem concerning using multiple constraint points to verify whether a particular treatment plan would produce an *NTCP* of approximately 5% was first examined by Stavrev *et al* (2). MATLAB was used in conjunction with Monte Carlo methods to produce integral DVHs and analyze their *NTCP* distributions. The methods used by Stavrev *et al* to create integral DVHs are discussed in the next section. The definition of integral DVHs was given in Section 1.2.

3.3.1 Original Algorithm for DVH Sampling

The first point of the volume array would have an initial value starting at zero, and the next point would be selected randomly (between 0 and 1), and would only be accepted if it was higher than the previous point. This would continue until it passed a threshold (0.999 in this case). The dose array would then be created of the same length, started and ending at 0 and 1 respectively, each interval uniformly spaced. The volume is then interpolated using another dose array from 0 to 1 with 0.01 increments, which gives all DVHs a constant length, and constant dose increments. This allows for easy averaging, though sacrifices diversification.

One drawback to this method is that it has a threshold of 0.999 to stop the process of creating a single DVH, which then takes an average of 1000 iterations per DVH. The number of points added to the DVH values is small in comparison to the number of iterations (average is ~9 points per DVH, maximum number of points ~23). In this method, most of the DVHs would populate the lower left quadrant of the plot area, which again limits the diversity of the DVHs produced.

This method of creating integral DVHs is acceptable for our purposes, however the method only has one source of randomness because it uses constant dose increments, A more robust method is thus required in order to produce as many diverse DVHs as possible, using at least 2 random variables.

3.3.2 Random Radial Distance and Angle Algorithm for DVH Sampling

The core purpose of our current developed program is to produce many diverse types of DVHs as efficiently as possible. Since integral DVHs can be represented by any

monotonically decreasing function (in the positive direction), there are many possible ways to approach this issue. However, as the quality of statistics improves with number of cases studied, calculation time becomes a limiting factor in the technique. The solution lies in the use of Monte Carlo methods, which enables diverse amounts of data to be created within a short amount of time.

Integral DVHs, as stated previously, are monotonically decreasing functions, where the x and y axis are represented by the integral Dose (Gy) and the Relative Volume irradiated, respectively. Given each DVH starts at [0,1] and ends at [1,0], hence are normalized on both axis, it is simple to modify the DVHs to have any maximum Dose. This gives flexibility to the program, as it can then be used to analyze any treatment plan. The method for creating integral DVHs is as follows. First, the initial coordinates are selected, at the point [0,1]. Then an angle and radial length are both selected randomly. These are used to calculate independent x and y increments for the next point. To maintain a monotonically decreasing function, the range is limited from 0 to $\pi/2$. The radial length is bounded by a maximum limit for each DVH. The next step is to subtract/add the respective increments from the previous point and add the new coordinate values to the array. This is repeated until either the x coordinate exceeds 1 or the y coordinate is below 0. See Fig. 3.1 for the first three steps of creating an integral DVH.

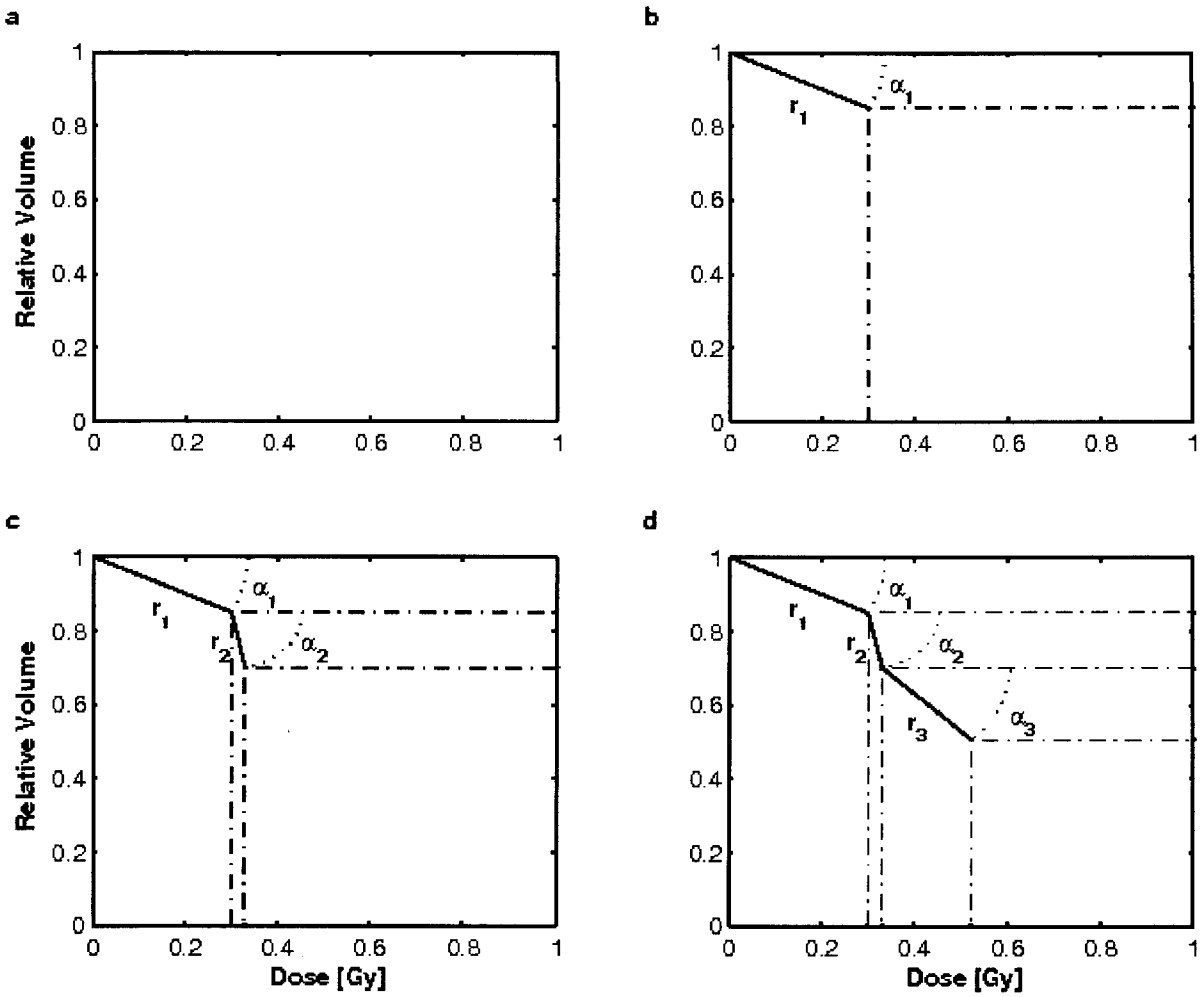

Figure 3.1 (a-d) Illustration of the random radial distance and angle DVH generating algorithm. The randomly selected radial distance and angle are selected by the r and α values respectively.

One problem with this particular method is that on average, the DVHs will tend to be close to the diagonal line, which is due to the randomness of the angle (which when

averaged over many values, equates to half the range, $\pi/4$). This is even more evident with DVHs that have a smaller maximum radial step size, resulting in an increase in increments, tends to vary only slightly from the diagonal in comparison with larger step sizes. This problem shouldn't be solved by only selecting large maximum radial step sizes, as this limits the number of points in each DVH, especially since they tend to cross either the x or y border quickly. However, despite the sacrifice to the number of points, larger step sizes do create DVHs that dramatically deviate from the axis far more often.

A second problem that occurs with this algorithm is that it doesn't produce many DVHs which cross the diagonal unless they are particularly close to it already. This is an unfortunate result of having a maximum random step size. As probability of choosing an angle close to either 0 or $\pi/2$ is slim, combined with an upper limit to the radial length, it is rare to see any DVH which crosses the diagonal. For future study, the use of a normal distribution instead of a uniform distribution could help resolve this issue when selecting radial length for each point. The low (but existent) probability of step sizes beyond the maximum radial step size would encourage more DVHs which would deviate significantly from the diagonal.

3.3.3 Methods to Increase Diversification of Potential Integral DVHs

3.3.3.1 *Varying Maximum Radial Step Sizes*

One way of varying potential DVHs is to ensure that each DVH has a different maximum radial length. This is achieved by selecting the maximum radial length randomly from a range of possible radial lengths, ranged between a minimum and maximum value. There must be a minimum value for the radial length for two reasons.

First, if the radial length is close to zero, the time to produce a single DVH will be very large and counter-productive as there is no need for thousands of points. Secondly, as stated before, the DVH produced will essentially be a diagonal line, or very close to it. The maximum radial length enables more deviating DVHs to be produced, but must be within limits to ensure each DVH has a minimum number of points. On average, each DVH should have ~70 points. Figures 3.2 (a) and 3.2 (c) demonstrate the differences between small and large step sizes respectively.

3.3.3.2 *Angle Weighting*

Given the problem of DVHs centering around the diagonal, a method to spread the DVHs was needed. Simply using large maximum radial lengths solves the problem but limits the number of points, and the quandary is still present for smaller radial lengths. One answer lies in weighting of certain ranges of angles so the mean angle is not $\pi/4$. However, this would create a new problem if the mean angle was simply changed from $\pi/4$ to another value, as the DVHs would then cluster around that value instead. It is desired that the spread of DVHs, and thus diversity, be increased; yet that the mean DVH curve be maintained as the same value for a uniform distribution of angles, which is a diagonal line from [0,1] to [1,0].

These issues are solved by using a randomly roaming weighting of a segment of the normal angle range. A certain angle range (or wedge if viewed radially), θ, is overlaid on top of a segment of angles anywhere within the normal range of angles (0 to π /2). Any angle values under this range covered by the wedge will be 1.5 times more probable of being selected than angles which are not within that segment. For each new DVH, the segment of angles of which the wedge overlays is randomly chosen. This new

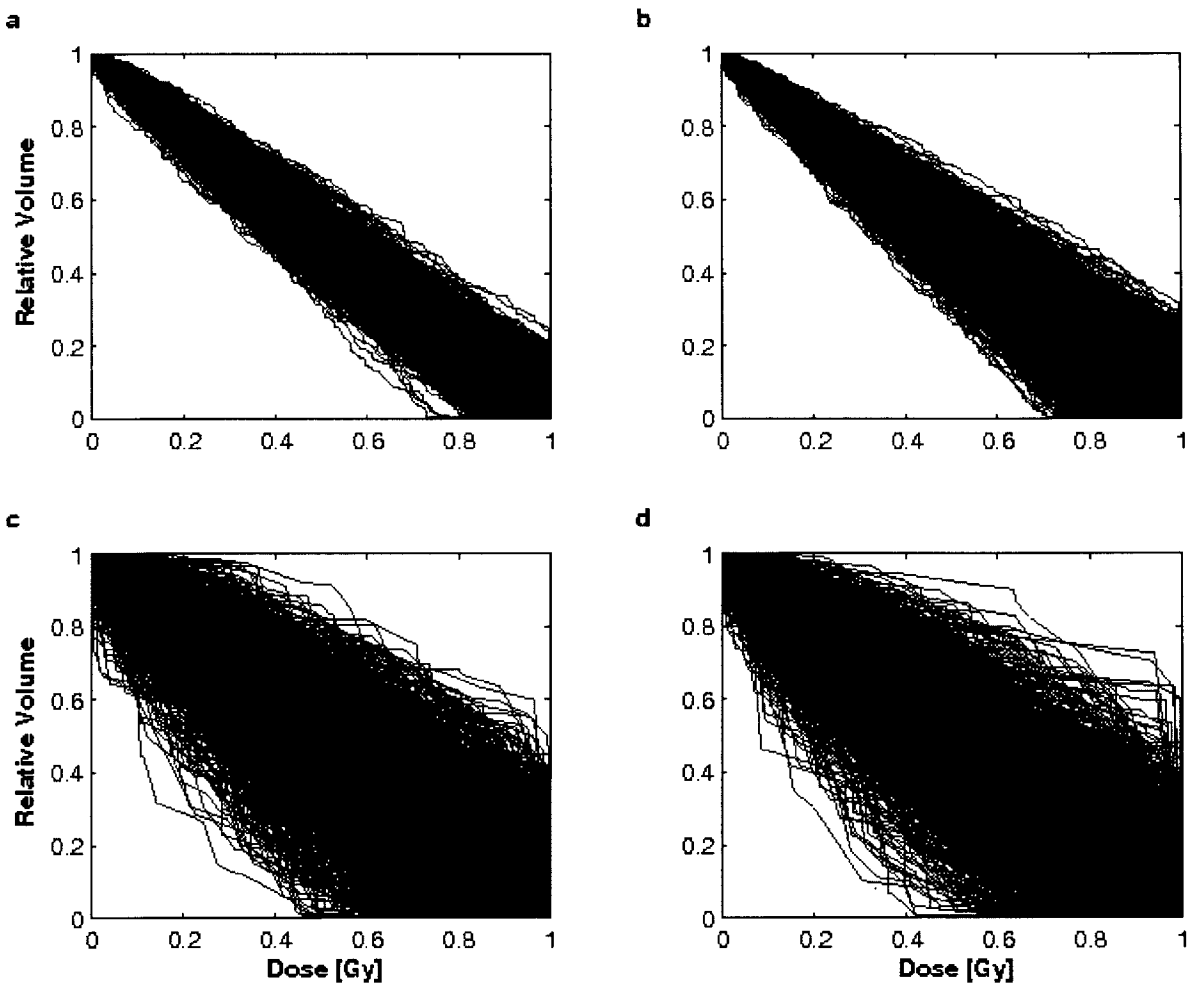

Figure 3.2 Example of 2000 random DVH samples created with: **(a)** small step sizes and uniform angle distribution, **(b)** small step sizes and weighted angle distribution, **(c)** large step sizes and uniform angle distribution, **(d)** large step sizes and weighted angle distribution.

method for determining angles is easily described by the following probability distribution

$$P(x,\theta,\phi)=\begin{cases} 0\le x<\phi & =\dfrac{2}{\pi+\theta} \\ \phi\le x<\phi+\theta & =\dfrac{3}{\pi+\theta} \\ \phi+\theta\le x\le \pi/2 & =\dfrac{2}{\pi+\theta} \end{cases} \tag{2.4}$$

where x is any angle between 0 and $\pi/2$, and φ is the angle at which the wedge starts, where φ ranges from 0 to $\pi/2$-θ. In comparison, the normal distribution of angles is given by $P(x)=\frac{2}{\pi}$, $\forall x \mid 0 \le x \le \pi/2$. φ is selected randomly for each new DVH, which varies where the wedge lies. θ can be any angle value within the normal range of angles.

This new probability distribution results in a variation of the angles mean values. Given a normal distribution, the mean angle $\bar{x}$ would be $\pi/4$, where the mean angle is given by a range of values, which are linearly dependent on φ. For example, if given $\theta=\pi/4$, then the range of mean angles is given by $\left(\frac{\pi}{4}\right)\frac{9}{10}\le\bar{x}\le\left(\frac{\pi}{4}\right)\frac{11}{10}$. By varying φ, the mean angle will change. To prove statistic merit of this new distribution, it can be mathematically proven that if the mean angle values are averaged over all possible values of φ for any given θ, the result will be $\pi/4$, independent of θ. Providing enough samples, it will converge to the same mean as given by the normal distribution.

By taking the derivative of $\bar{x}$ $\left(\bar{x}=\int_0^{\pi/2} xP(x,\theta,\phi)dx \Big/ \int_0^{\pi/2} P(x,\theta,\phi)dx\right)$ over θ, and letting φ = 0, it can be shown that the best wedge angle is given by $\pi\left(\sqrt{6}-2\right)/2$ (or

0.4495π). It produces the range $\pi\left(\sqrt{6}-2\right)/2 \le \bar{x} \le \pi\left(3-\sqrt{6}\right)/2$ (or $0.4495\pi \le \bar{x} \le 0.5505\pi$).

Given these additions to the code, the DVHs could deviate more from the diagonal and thus more varied DVHs would be produced. In total, the additional calculations are minimal and are proportional to the number of DVHs created. The calculation time is small if compared to any of the more complicated methods of determining radial length or angle weighting, as they would either add extra calculations per point created, or many more calculations per DVH. Figure 3.2 (a) and 3.2 (b) show the difference of using a uniform angle distribution and the new angle distribution, respectively, for small step sizes. Figures 3.2 (c) and 3.2 (d) show the difference of using a uniform angle distribution and the new angle distribution, respectively, for large step sizes. This is more difficult to see than in Figs 3.2 (a) and 3.2 (b) (as the increase in DVH-space is relatively larger), though it can be seen that the DVH-space is slightly wider in Fig 3.2 (d) than in Fig 3.2 (c).

To reiterate, each DVH created has a maximum radial length and individual weighted angle distribution, which are chosen randomly yet remain constant for that individual DVH.

3.3.3.3 *Partial Organ Irradiation*

The two examples given for DVH generation only cover non-homogenous distribution of dose in the organ volume. As there are cases where some parts of an organ will receive all or zero of the total administered dose (eg: partial organ irradiation), this needs to be considered.

Thus, for some of the DVHs created, the initial relative volume value (which normally begins at 100% for 0 Gy) was varied in order to represent volumes where segments were not irradiated at all. In order to represent DVHs which had segments that had received 100% of the dose, the relative volume was kept at 100% up to X dose, where X was a varied percentage of the total dose. Organs which had a portion receive the same maximum dose as the tumour would produce DVHs such as those. Most potential DVHs can be generated by allowing for both of these possibilities.

3.3.4 Calculating Constraints from DVH/NTCP Data

The next step in the program is to calculate the *NTCP* values for each integral DVH. Previous to any calculations, a particular organ to be examined must be selected. Each organ is different in their structure and reaction to radiation (both physical and temporal), so they will have different NTCP parameter values. These parameters are stored in text files to facilitate access. They are retrieved when an organ is selected. Most of the Lyman parameters were derived (4) from the Emami *et al* data, which has no confidence intervals for its values of tolerance doses. There are some parameters though which were obtained from other sources (5-12) that do have confidence intervals, though currently the program does not take these into consideration. The Lyman model parameters D_{50}, n and m are given for a multitude of organs. The population based critical volume model parameter values are also derived from the Emami *et al* data, giving values for D_{50}, γ_{50}, μ_{cr} and σ (3).

3.3.5 Scaling of Generated DVHs

The NTCPs cannot be simply calculated from the integral DVHs that are generated. There are two steps to take beforehand, the first being multiplying the relative dose points by an absolute maximum dose value.

By definition, the relative dose has a maximum value of 1 and is unitless. We could very well use the relative dose to calculate the *NTCP*, however, it would make little sense as it would be assuming that the maximum dose has a value of 1 Gy. In order to produce meaningful NTCPs, we must have sensible dose values in the DVHs. This is simply achieved by scaling the relative dose values by an absolute maximum dose value. Of course these values will vary depending on the organ and treatment protocol in question.

Clinically, the maximum dose that a particular organ can receive can vary depending on where the planning target volume (PTV) is located in relation to the organ in question, and the maximum dose prescribed to the PTV. In order to cover most possibilities, a range of maximum doses is required. It is most desirable to use the dose for 99% *NTCP* and 5% *NTCP* for the maximum absolute dose value, D_{max}, and the minimum absolute dose value, D_{min}, respectively. These *NTCP* values would be calculated using a uniform irradiation of the entire organ at the mentioned dose values. The maximum dose value that the relative dose of the k^{th} DVH created is multiplied by is given by

$$D_{\max,k} = D_{\min} + n_k \left(D_{\max} - D_{\min} \right) \tag{2.5}$$

where n_k is a random number generated from a uniform distribution. D_{max} and D_{min} values have to be calculated for both the Lyman and the CV models, for each organ in question.

Alternatively, it is possible to use the clinically absolute maximum and minimum values of the highest dose a normal tissue has been subject to for D_{max} and D_{min}, respectively. Despite that using the clinical values would cover most clinically feasible variations of dose distribution, statistically and logistically it makes sense to favour the calculated values instead. It should be noted that in some cases, the calculated and clinical dose values can be quite varied. The clinical D_{min} can potentially be zero, as the organ can receive no dose whatsoever during an irradiation treatment (being outside the radiation field). Comparably, the D_{max} for some organs can be quite high, receiving almost the total prescribed dose meant for the tumour (as such is the case for healthy lung tissue in lung tumour treatments).

Given all possible relative DVHs, if the D_{max} is too high, most calculated *NTCP* values will be 100% or very close. If the D_{max} is too low, many intermediate *NTCP* values will be missed. The same applies for D_{min}, though in reverse. Too small a D_{min} value will result in very low, close to 0% *NTCP* values, while too high a D_{min} could potentially omit *NTCP* values that we are trying to study. In one case, large D_{min} or small D_{max} values could eliminate potential *NTCP* values in either the lower or upper limits respectively. But if there are too many DVHs, which are producing 0% or 100% *NTCP* values (because of low D_{min} or high D_{max} values respectively), the reduction of DVHs with intermediate *NTCP* values could create a bias. As we are interested in all intervals of *NTCP* (intervals are 0-10%, ..., 90-100%), neither of these situations are desirable.

Using 99% *NTCP* as an upper limit for calculating D_{max} promotes more varied *NTCP* values in the DVHs produced. Using 5% *NTCP* as the lower limit for calculating D_{min} ensures that most DVHs will not result in very low, near-zero *NTCP* values. Hence calculated D_{max} and D_{min} values are preferred instead of clinical values.

The second step involves calculating the differential DVH from the integral DVH. The integral DVH shows how much dose is received by at *least* a certain percent volume of the organ in question. However, this is not useful for calculating *NTCP* values, which require exactly what dose each section of the organ received. Thus the integral DVH must be differentiated before any *NTCP* can be performed. See Section 1.2 for definitions of integral and differential DVHs.

3.3.6 NTCP Calculating/Averaging and Binning of Integral DVHs Based on NTCP

Two different models are used to determine the *NTCP* values: the Lyman model (see Section 1.6.7) and the Critical Volume Model (see Section 1.6.8). Once a DVH is created, the *NTCP* using both models is calculated, and the DVH is named and saved as well as its *NTCP* values. To graphically visualize this, Fig. 3.3 represents the histograms of the *equivalent uniform dose* (EUD) and *NTCP* values that are created for a random sampling of DVH curves. The EUD is essentially the same as the GMD, given by Equation **(1.25)**. Figure 3.3 (a) demonstrates the distribution of the EUD for the randomly generated DVH curves and Fig. 3.3 (b) illustrates the distribution of the *NTCP* values resulting from the distribution of EUD values in Fig. 3.3 (a).

For both NTCP models, the DVH is sorted into the following bins based on their *NTCP* values: 0-10%, 10-20%, 20-30%, 30-40%, 40-50%, 50-60%, 60-70%, 70-80%, 80-90%, 90-100%, and 4.5-5.5%. Each DVH has its Relative Volume interpolated using an

equally spaced Percent Dose array. Depending on which bin(s) the DVH lies within, the new Relative Volume array is then added to the previous values. After all DVHs have been calculated, the summed Relative Volume arrays for each bin are divided by the total number of DVHs sorted per bin, thus creating the average DVH for each bin.

3.3.7 Calculating Dose Volume Constraint Values

The averaged DVHs correlating to each range can now be used to calculate Dose Volume (DV) constraints. Given that *NTCP* values around or below 5% are acceptable

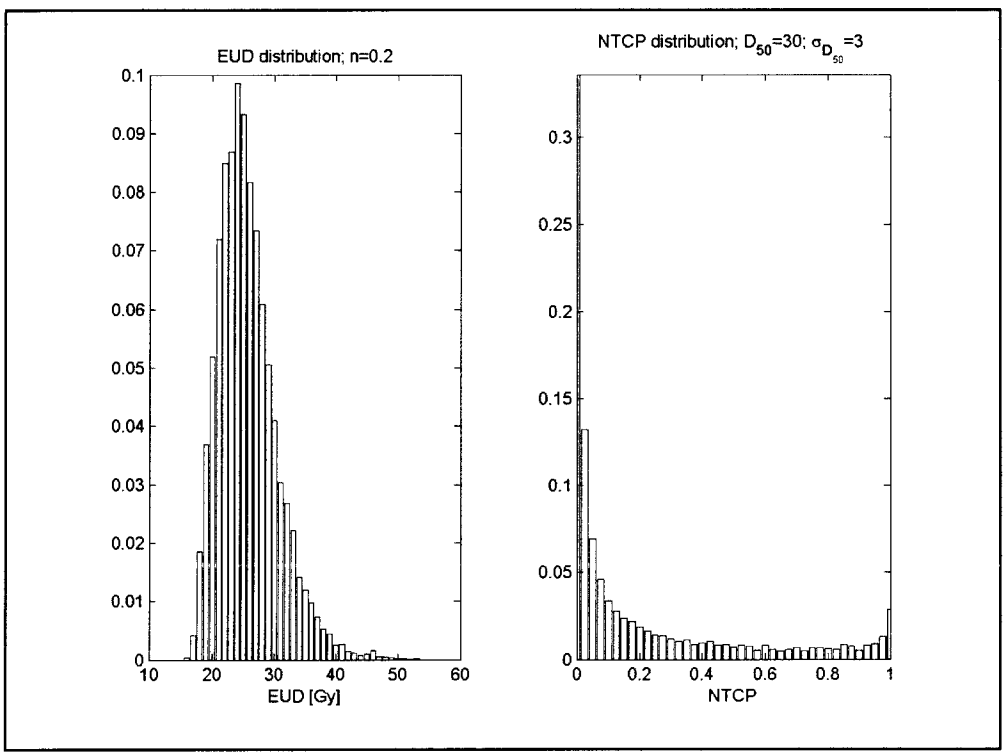

Figures 3.3 (a) and **(b)** Histogram of *EUD* and *NTCP* values respectively, derived from randomly generated DVH curves.

in radiotherapy treatments, that particular range was examined. Any *NTCP* values above 5% would not be of interest as those values would not be acceptable in any radiotherapy application. On the other hand, values much below 5% would skew the averaged DVH as there are many more possible DVHs that would equate to almost zero or zero *NTCP* than to 5+/-0.5%.

The DV constraint points for the *NTCP* range of 5+/-0.5% are calculated by first creating a Relative Volume array with 0.1 spacing between each point (0.1, 0.2, ... 0.8, 0.9). The average DVH value for the 5+/-0.5% bin is then used in conjunction with the new Relative Volume array to interpolate the corresponding Percent Dose points. This new array now represents the 5+/-0.5% *NTCP* constraint points for that particular organ.

3.3.8 DVH Probability of Satisfying Calculated DV Constraints for 5+/-0.5%*NTCP*

The program then takes all the DVHs that had *NTCP* values within the 5+/-0.5% range, and determines whether each of the DVHs satisfies the given constraints. A DVH satisfies the DV constraints if the difference between it's own Relative Volume values corresponding to the 5+/-0.5% constraint values and the Relative Volume array used to produce the constraint points are less than or equal to the tolerance value ε. For each DV constraint point (9 points in total), it tallies how often each DVH satisfies the constraint in question. The percentage of total DVHs that satisfies the 5+/-0.5% *NTCP* constraint points can then be calculated.

3.3.9 Determination of *NTCP* Distribution for Calculated Constraint Values

While finding the constraints is an important part of this research, it means little if the DVHs that satisfy the constraints differ from the normal 5+/-0.5% *NTCP* range. This last part of the code tends to that issue.

Each DVH that was created is loaded. Using the same method as is mentioned in the previous section, all DVHs are compared to the DV constraints for 5+/-0.5% *NTCP*. If the constraints are satisfied, the DVHs are tallied into equally spaced bins depending on their *NTCP* value for each model. This determines what the ranges of *NTCP* values that can satisfy the constraints are.

3.4 *Results*

We used the liver as the organ for our calculations to date, thus setting the parameters for the NTCP models. D_{min} and D_{max} for the Lyman model were 30.1 and 54.0 Gy respectively. D_{min} and D_{max} for the CV model were 30.2 and 52.0 Gy respectively. Results are displayed graphically in Figs. 3.4 and 3.5. In order to produce enough diverse samples to study, the two DVH generators were used in conjunction with each other.

Figure 3.4 displays the average integral DVHs corresponding to the first six bins ([0%, 10%], [10%, 20%], [20%, 30%], [50%, 60%], [70%, 80%] and [90%, 100%]) denoted in Section 3.3.6. The numbers in the legend relate to the bins, so 1 = 0-10%, 2 =10-20% and so forth. Figure 3.4 (a) and 3.4 (b) denote the Lyman and CV NTCP model respectively.

From Fig. 3.5, we can see a plot of the DVH curves that lie within the 5+/-0.5% *NTCP* range. In black, we see the constraint points that were calculated from the average DVH for the same *NTCP* range, which were interpolated from the average of the DVHs

inside the 5+/-0.5% *NTCP* range (using a constant incremented volume array). Figure 3.5 (a) and 3.5 (b) denote the Lyman and CV NTCP model, respectively. Overlaid on top of plots are the Emami *et al* (1) tolerant doses for 5% complication within 5 years.

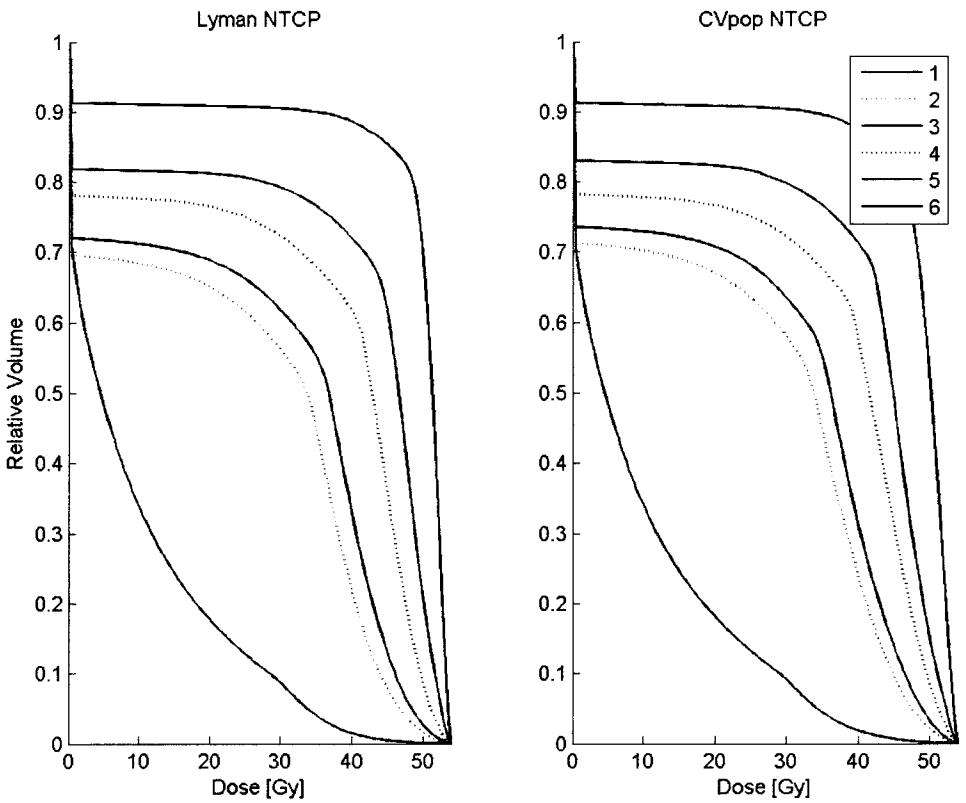

Figure 3.4 (a) and **(b)** Average DVH curves based on the Lyman and CV (population) NTCP models respectively. The lowest volume to the highest volume curves (legend values 1-6) correlates to *NTCP* = [0%, 10%], [10%, 20%], [20%, 30%], [50%, 60%], [70%, 80%] and [90%, 100%].

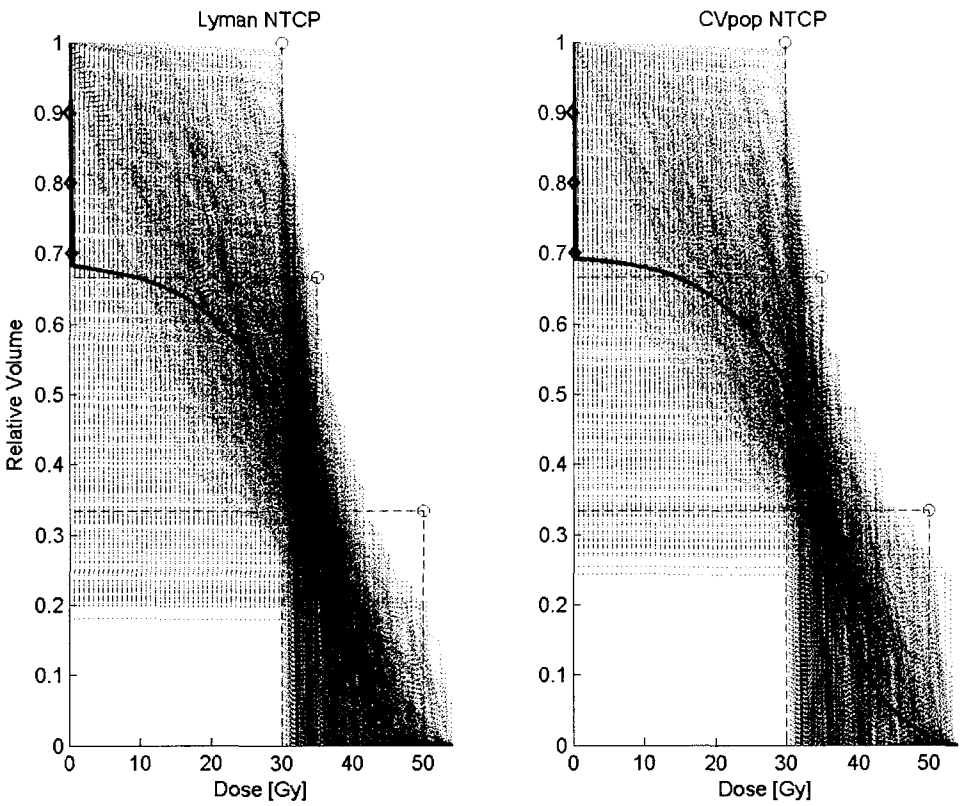

Figure 3.5 (a) and **(b)** Plot of DVH curves which satisfy the *NTCP* range of 5.0+/-0.5% *NTCP* for the Lyman and CV (population) model respectively, for the liver. The black curve represents the average DVH for the range of 5.0+/-0.5%, the black dots representing the calculated constraint points. The red circles and dashed lines represent the Emani *et al* DV constraint points for the liver.

Figure 3.6 demonstrates the distribution of the *NTCP* of all DVHs which satisfy the ε criteria dictated in Section 3.3.9, though only for the constraint point with the volume % value of 0.2. Figure 3.6 (a) and 3.6 (b) denote the Lyman and CV NTCP model respectively.

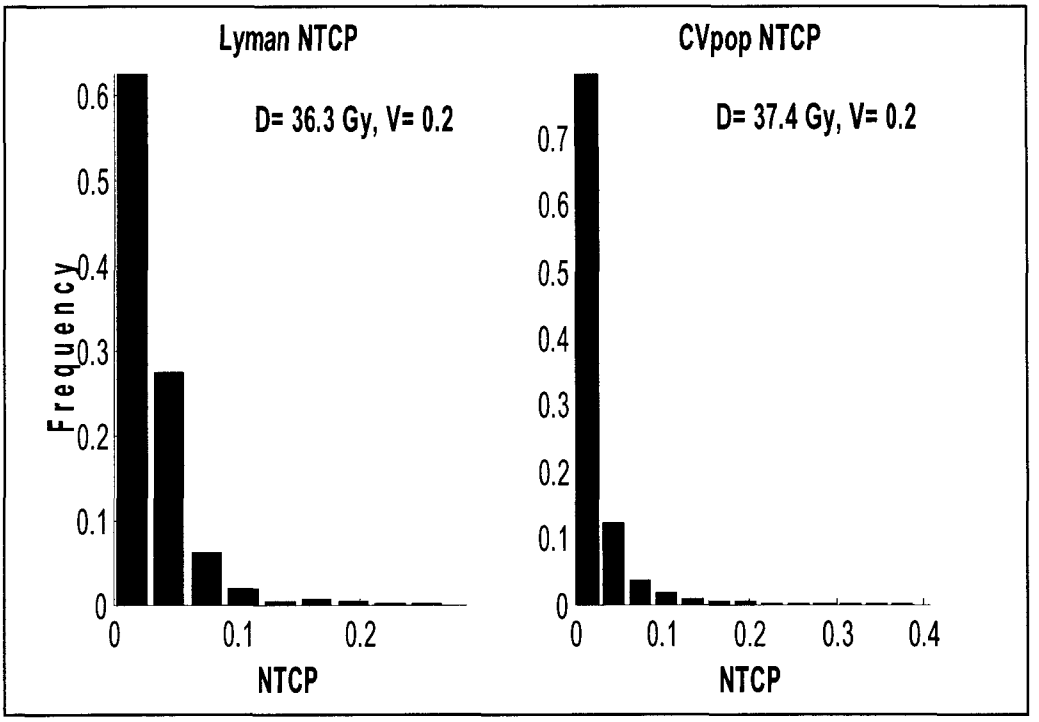

Figure 3.6: Distributions of all DVHs which satisfy the ε-criterion for both NTCP models. The DVHs that pass within the ε of the V=0.2 constraint point defined by the averaged 5% *NTCP* are distributed by their *NTCP* values.
Left: Lyman NTCP distribution - constraint [36.7 Gy, 0.2];
Right: CV population NTCP distribution - constraint [37.9 Gy, 0.2].

3.5 *Discussion*

It is interesting to note in Figs. 3.4 (a) and (b) that all of the curves are similar in shape, except for the one representing the bin 0-10% *NTCP*. The 0-10% *NTCP* curve, instead of having a negative curvature, has a positive curvature, and does not level off before dropping to the point [1,0], but instead curves down almost exponentially. This dramatic difference of shape, despite the same width in *NTCP* range, can be explained by examining the bounds of *NTCP*, in particular the lower bound.

The NTCP models that were used in the program are based on error functions (the generalized error function is given by $erf(z) = \frac{2}{\sqrt{\pi}} \int_0^z e^{-t^2} dt$). Because of this, there will exist a wide range of dose and relative volume values where no or negligible complication will be shown, while the number of DVHs that would give non-zero complication probabilities are much less common in comparison. This can be easily seen in Fig. 3.3 (b), which shows significantly more low *NTCP* values in the distribution than compared to the medium range. Of course, it cannot be ignored that the *NTCP* distribution is dependent on a number of factors. These are the maximum dose that is chosen to be studied, as well as the quality of the DVHs produced (uniformly varied over all possible DVH curves), which is dependant on the DVH algorithm generator. However, providing that enough uniformly varied DVHs were produced (i.e. there is no bias or weighting given to the curves), this will be true. Thus, for the curve representing 0-10% *NTCP*, it is heavily weighted towards *NTCP*~0, which is reflected in the shape of the curve.

If we now compare the curves related to 5+/-0.5% *NTCP* in Fig. 3.5 to those in Fig. 3.4, it can be seen that the 5+/-0.5% curve would lay directly between the 0-10% and 10-20% curve. As the 5+/-0.5% does not include 0% *NTCP*, it is not weighted as the 0-10% curve and thus can be seen to mimic the shapes given by the rest of the curves (2-6) in Fig. 3.4.

It is interesting to note how, in Figs. 3.5 (a) and 3.5 (b) there exists a rectangular region in which no DVH curves pass through. In both Figures 3.5 (a) and 3.5 (b), it extends to 30 Gy along the x-axis, and to 0.180 and 0.243 along the y-axis respectively.

As 30 Gy is the defined tolerance dose (at 100% volume) for 5% complication, the fact that it marks the x-axis limit is not surprising.

Supposedly, this would mean that any DVHs that exist entirely inside this region would automatically be excluded from having an *NTCP* between 4.5 and 5.5%, and most likely would pertain to *NTCP* below 4.5%, for this particular maximum dose and organ. This is assuming that the DVHs that were sampled were diverse enough to cover this area in question. For alternative maximum doses, the upper limit for this rectangle (and perhaps shape) would fluctuate as less or more potential DVHs are included in the calculations. To determine the absolute limits of these regions, for a particular organ the maximum clinical dose allowed would have to be used. This, of course, is dependant on the mathematical models being used as well as the data which the parameters are based on.

Focusing on the upper left region of the plot area, we can see for both models that there is a definite curvature to the accumulative DVHs. The curvature has an exponential behaviour. This behaviour is reasonable for the Lyman model (see Section 1.6.7.2) because the tolerance dose at partial volume v is dependent on the v^{-n} (for liver n has the value of 0.32). This can be imagined if we assume a constant value for the *NTCP* (approximately 5%, though it can be presumed that most DVHs that touch the top left border would be closer to 5.5%). Because of the inverse exponential relation of v versus n, as the dose decreases, the partial volume increases accordingly.

In fact, by imagining a set of DVHs which have constant dose up to a certain relative volume, it could be easily seen that they would outline the barrier perfectly (see Fig. 3.7). Any DVH with points beyond the barrier would result in an *NTCP* higher than

5.5%. If we use the same reasoning concerning the CV model, and assume constant dose up to a certain partial volume, the relationship between the two variables is very similar to their relationship in the Lyman model. Thus it is not surprising that the border governing the upper left portion of the plot is of similar exponential shape. We can make these assumptions of constant dose and partial volume to represent the outer border of DVHs that satisfy the models, as they represent the maximum values possible for any DVH that exist within the set *NTCP* range.

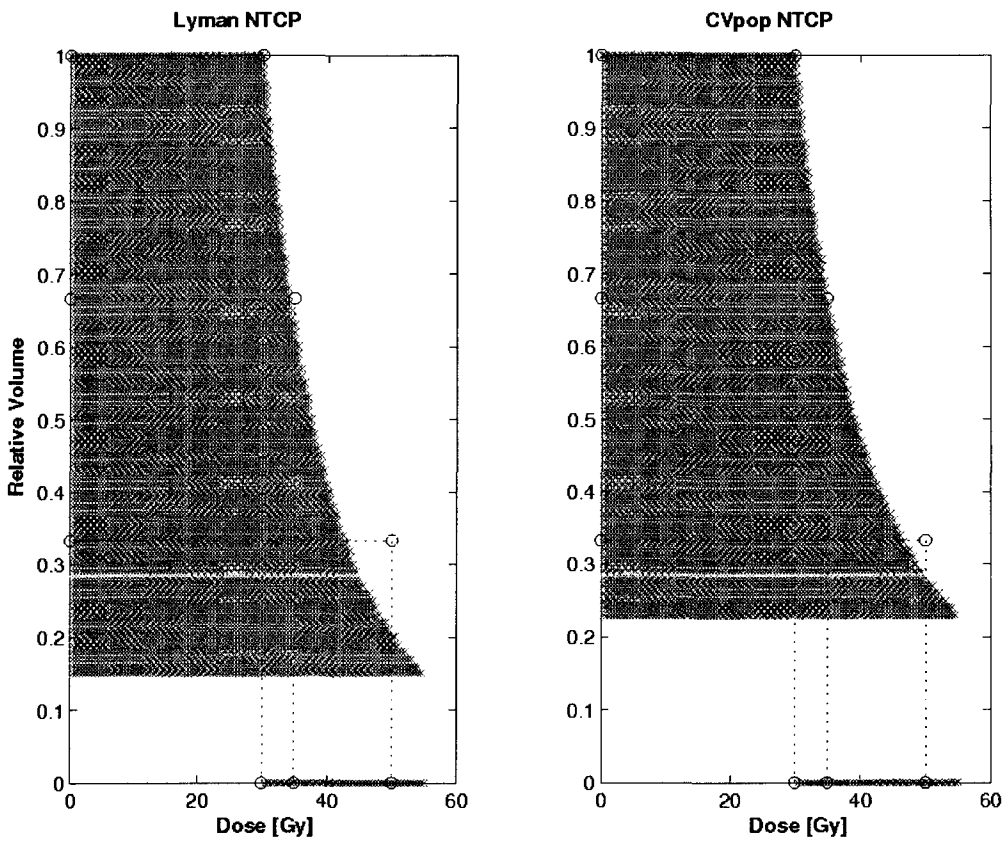

Figure 3.7 (a) and **(b)** Displays constant dose DVH curves which are within the range of 5.0+/-0.5% NTCP for both Lyman and CV models respectively, for the liver.

It is interesting to note that in both models, the Emami *et al* constraint points for 5% complication probability for whole and 2/3 partial volume are bridged by the DVH functional space, but no DVH ventures close to the 1/3 partial volume constraint point. Any DVH with points above or to the left of these constraint points (positive volume or dose direction only) would be classified as having a larger value of *NTCP* (as *NTCP* increases with dose and partial volume). Therefore, it is not surprising that the DVH upper border runs close or through these constraint points, though the fact that the 1/3 partial volume constraint is very far away from the border may warrant further study.

As was stated previously in the introduction to this chapter, the Emami *et al.* DV constraints can only be used individually, as a single dose per partial volume point, and cannot be combined together, because this would create larger NTCPs than those predicted.

We can observe from Figs. 3.5 (a) and 3.5 (b) that many DVHs exist below these constraint points, all with NTCPs that are within 5+/-0.5%. This is, however, not a guarantee that any DVH below these points will be within or even below this range. A DVH simply containing any two of the Emami *et al.* constraints would prove this. By averaging the DVHs, it is theorized that their average will produce a potential base-line for DVHs. The possible *NTCP* values can then be assessed from the DVHs. A question lies in how accurate these new constraint points could be. It is important that the averages and constraint points not be misinterpreted.

One key point that must be taken into account is that the DVH functional spaces given different *NTCP* ranges will overlap on top of one another. In other words, the same point that exists in a DVH that produces a 0% *NTCP* could also exist in a DVH that

produces a 100% *NTCP*. Thus if we look at Fig. 3.5, we cannot assume that any DVH that lies within the area containing the DVHs will produce a DVH within the range that governs those DVHs. This is explicitly shown by the results of the *NTCP* values for the calculated constraints. The desire however, is to find constraint points where the DVHs within a tolerance value of them will produce consistent *NTCP* values within (or below) that range.

For both sets of constraint points, the *NTCP* was calculated with the respective models for each set. The constraints generated using the Lyman model and CV model produced an *NTCP* of 4.98% and 4.97%, respectively. These values not only lie within *NTCP* range examined for those constraints, but are very close to the median value of 5%.

Examining the DVH generators, it should be considered that both of the methods mentioned (see Sections 3.3.2 and 3.3.3) have their disadvantages. Both generators have locations on the plot area where DVHs produced are likely to inhabit. This will not affect the *NTCP* values of the DVH, however, it will skew the average DVH for any range of *NTCP* values. It is in the best interests for future study that distributions of DVHs which are more uniform be developed to produce more accurate average DVH curves, and thus potential constraint points for inverse treatment planning.

3.6 *Conclusion*

As stated previously, the combination of the three Emami *et al.* DV constraint points (for 5% *NTCP*) are not a good basis for determining the merits of a DVH. In fact, for the DVHs examined, there was no DVH that even contained the 1/3 partial volume constraint point at all for the range of 5+/-0.5% *NTCP*. There exists potential for these

new constraints in inverse treatment planning, though more study is needed into how these constraints reflect the DVHs used to produced them. More uniform DVH sets are required to increase confidence in the average DVH curves and calculated constraint values.

Regardless of the constraint points, Figs. 3.5 (a) and (b) show that there are regions where, if all of the points of any DVH lie within this area, the *NTCP* will be almost guaranteed to be either above or below the upper or lower *NTCP* range, respectively. Providing diverse enough DVH sets are evaluated, the confidence in these regions will improve.

It cannot be forgotten that the Emami *et al.* constraint points are based on clinician's opinions and experience, not on scientific data. Since the parameters from which the NTCP models rely on for each organ are derived from this data, the accuracy of these models to give reliable complication probabilities comes into question. However, if faith is to be given to the Emami *et al.* data, the calculated constraint points found through this work will be a vast improvement from using the original constraint points themselves.

3.7 *References*

1. Emami B, Lyman J, Brown A, Coia L, Goitein M, Munzenrider JE, et al. Tolerance of normal tissue to therapeutic irradiation. Int J Radiat Oncol Biol Phys 1991;21(1):109-22.

2. Stavrev P, Stavreva N, Hristov D, Fallone B. Reverse Mapping of Normal Tissue Complication Probabilities onto Dose Volume Histogram Space: Problem Formulation, Illustration, and Implications. In: Proc. of World Congress on Medical Physics and Biomedical Engineering; 2003, 24 - 29 August; Sydney, Australia; 2003, 24 - 29 August.

3. Stavrev P, Stavreva N, Niemierko A, Goitein M. The Application of Biological Models to Clinical Data. *Phys Medica* 2001;XVII(2):71-82.

4. Burman C, Kutcher GJ, Emami B, Goitein M. Fitting of normal tissue tolerance data to an analytic function. Int J Radiat Oncol Biol Phys 1991;21(1):123-35.

5. Moiseenko V, Craig T, Bezjak A, Van Dyk J. Dose-volume analysis of lung complications in the radiation treatment of malignant thymoma: a retrospective review. Radiotherapy and Oncology 2003;67(3):265-274.

6. Dawson LA, Normolle D, Balter JM, McGinn CJ, Lawrence TS, Ten Haken RK. Analysis of radiation-induced liver disease using the Lyman NTCP model. International Journal of Radiation Oncology Biology Physics 2002;53(4):810-821.

7. Cheng JCH, Wu JK, Huang CM, Liu HS, Huang DY, Cheng SH, et al. Radiation-induced liver disease after three-dimensional conformal radiotherapy for patients with hepatocellular carcinoma: Dosimetric analysis and implication. International Journal of Radiation Oncology Biology Physics 2002;54(1):156-162.

8. Seppenwoolde Y, Lebesque JV, de Jaeger K, Belderbos JSA, Boersma LJ, Schilstra C, et al. Comparing different NTCP models that predict the incidence of radiation pneumonitis. International Journal of Radiation Oncology Biology Physics 2003;55(3):724-735.

9. Martel MK, Sahijdak WM, Ten Haken RK, Kessler ML, Turrisi AT. Fraction size and dose parameters related to the incidence of pericardial effusions. Int J Radiat Oncol Biol Phys 1998;40(1):155-61.

10. Kwa SL, Theuws JC, Wagenaar A, Damen EM, Boersma LJ, Baas P, et al. Evaluation of two dose-volume histogram reduction models for the prediction of radiation pneumonitis. Radiother Oncol 1998;48(1):61-9.

11. Eisbruch A, Ten Haken RK, Kim HM, Marsh LH, Ship JA. Dose, volume, and function relationships in parotid salivary glands following conformal and intensity-modulated irradiation of head and neck cancer. Int J Radiat Oncol Biol Phys 1999;45(3):577-87.

12. Roesink JM, Moerland MA, Battermann JJ, Hordijk GJ, Terhaard CHJ. Quantitative dose-volume response analysis of changes in parotid gland function

after radiotherapy in the head-and-neck region. Int J Radiat Oncol Biol Phys 2001;51(4):938-946.

Chapter 4

Conclusion

By definition, radiobiology is the study of the effect of radiation on living organisms. Mathematical models based on the principles of radiobiology are very important for understanding the underlying mechanisms involved with how either tumour cells or normal tissues react to radiation damage, as well as possibly predicting more tailored maximum and minimum dose tolerances. However, data is difficult to produce or acquire for various reasons. Obvious ethical issues do not allow testing to be done on humans. While animal testing certainly enables a better understanding of radiobiological processes, it doesn't unequivocally lend how radiation affects human tumours and tissues. However, it's difficult to get statistically significant amounts of data for tumour effects, and is not very useful for examining NTCP models. Comprehensive databases of patient treatment plans and health after treatment would provide a great asset for determining more accurate tolerance dose values to normal tissues, though would require global participation and many years to develop enough data. *In vitro* data is less labour intensive to acquire than *in vivo*, however it limits itself to tumour cell studies. Additionally, by definition, the data concerns cells in an artificial environment, though it is still useful to understand the underlying elements of tumour response to radiation. How much can we rely on the *in vitro* assay? The connection between *in vitro* and *in vivo* studies is not clear at this moment; and, in practice, *in vitro* data may add even more uncertainties under certain circumstances. In the instance of prostate cancer, for example,

as pointed out by Wang *et al.* (1), the differences between *in vitro* data reported from different labs are as large as, or even larger than, the differences observed among various cell lines.

Over the past decades, radiation therapy for cancer treatment has improved constantly. The invention of the CT scanner, multileaf collimators and tomotherapy have all been steps forward to accurately tailor the dose administered to the tumour during therapy. Yet, by the nature of radiation it is impossible to completely spare all healthy tissue for any treatment, despite these efforts. Inverse planning was developed in order to try to maintain proper dose coverage of the tumour, but spare any healthy tissue. However, without study of how tumours and normal tissues are affected by radiation quantitatively, inverse planning becomes inane. Given this, radiobiological models and methods are becoming of more interest, despite the limited data to base them on.

Both experiments involving *in vitro* and *in vivo* data are important in efforts to understand the effects of radiation on tumour cells. In Chapter 2, *in vitro* data from Tarnawski *et al* (2) was used to examine several different TCP models (see Section 2.2.1). The data consists of two cell lines which were irradiated using several different fractionation schemes. The best fits are those which use the LQ model in conjunction with repopulation. Other models had similarly good fits, though they were dismissed as the calculated parameters were irregular. Previous research (3) which focussed on *in vivo* data using the same models found that a single hit model with repopulation fit the data better. However, given later work (4), it is hypothesized that the LQ model could correspond to both *in vivo* and *in vitro*. By better understanding these models and data,

hopefully they will be able to improve current clinical techniques by being able to more accurately tailor dose distributions.

Recommendations for future work consist of suggesting experiments which have more diverse multiple fractionation schemes. Models which did not have immediate repair tended to not be represented well by the data, with the exception where the other parameters were irregularly adjusted to compensate for the presence of non-instantaneous repair. Considering that the data had, at minimum, a single day between fractions, this is not surprising. Data using fraction separation times which more closely related to those observed in the laboratory, should be used to examine the mathematical descriptions of cell repair.

However, despite improving our knowledge of tumour cell death, there is no avoiding radiation damage to healthy tissues. It is unwise to strictly focus on tumour control models and neglect how radiation would affect normal tissues, as the entire reason for curative (as opposed to palliative) treatment is to maximize tumour cell death while minimizing healthy tissue damage, whether immediate or long term. Thus from Chapter 3, we discuss potential ways to improve modern clinical methods of determining NTCPs from clinical DVHs.

A very important issue in contemporary inverse treatment radiotherapy planning is the specification of proper dose-volume constraints limiting the treatment planning algorithm from delivering high doses to the normal tissue surrounding the tumor. Recently, a method called reverse mapping of normal tissue complication probabilities (NTCP) onto dose volume histogram (DVH) space, was proposed. This method allows the calculation of appropriate biologically based dose-volume constraints to be used in

the inverse treatment planning. The method of reverse mapping requires random sampling from the functional space of all monotonically decreasing functions in the unit square. In Chapter 3, we have concentrated on the development of the " Random angle - random step descent" method for DVH random sampling. DVHs were generated and their NTCPs were calculated for the liver. The parameters of the NTCP models were derived from the Emami *et al* (5) data, and new Dose-Volume constraints are derived and analyzed from the data produced, in particular the DVHs which produced *NTCP* values of 5±0.5%.

The Emami constraints were found to lie along the upper boundary outlined by the DVH subspace dictated by the condition *NTCP*=5±0.5%. Any DVHs which passed through a combination of the Emami constraints are outside the *NTCP* range of 5±0.5%. The *NTCP* of the calculated DV constraint points was shown to be within the same range which governed the DVHs that they were based on. Potentially, the constraints could be improved by developing more randomly uniform DVH generators to avoid bias.

Recommendations are for the development of more diverse and less location biased DVH generators so as to give more confidence in the calculated confidence values. Also, given that the Emami *et al* data is based mostly on physicians observations and not quantitative methods, not to mention that the data have no error governing the tolerance dose values, it could be helpful to find more statistically accountable tolerance dose values.

References

1. Wang JZ, Mayr NA, Li XA, Stewart RD. Modeling prostate cancer: In regards to Nahum et al. (Int J Radiat Oncol Biol Phys 2003;57 : 391-401). International Journal of Radiation Oncology Biology Physics 2005;61(1):309-310.

2. Tarnawski R, Widel M, Skladowski K. Tumor cell repopulation during conventional and accelerated radiotherapy in the in vitro megacolony culture. International Journal of Radiation Oncology Biology Physics 2003;55(4):1074-1081.

3. Stavreva N, Stavrev P, Warkentin B, Fallone BG. Investigating the Effect of Cell Repopulation on the Tumor Response to Fractionated External Radiotherapy. Med Phys 2003;30(5):735-42.

4. Stavreva N, Warkentin B, Stavrev P, Fallone BG. Investigating the Effect of Clonogen Resensitization on the Tumor Response to Fractionated External Radiotherapy. Med Phys 2005;in print.

5. Emami B, Lyman J, Brown A, Coia L, Goitein M, Munzenrider JE, et al. Tolerance of normal tissue to therapeutic irradiation. Int J Radiat Oncol Biol Phys 1991;21(1):109-22.

Bibliography

(page numbers in the brackets at the end of each entry identify the locations of each reference in the thesis)

Abramowitz, M. and Stegun, I. A. (1972) *Handbook of Mathematical Functions with Formulas, Graphs, and Mathematical Tables,*, New York: Dover. [page 24]

Archambeau, J. and Shymko, R. (1988) *Int. J. Radiat. Oncol. Biol. Phys.,* **15,** 727-734. [page 20]

Brahme, A. (1984) In *18th Use of Computers in Radiation Therapy*Totonto,Canada, pp. 269-74. [pages 15, 20, 33]

Brahme, A. and Agren, A. K. (1987) *Acta Oncol,* **26,** 377-85. [pages 15, 33]

Brenner, D. J. and Hall, E. J. (1991) *Br J Radiol,* **64,** 133-41. [page 14]

Burman, C., Kutcher, G. J., Emami, B. and Goitein, M. (1991) *Int J Radiat Oncol Biol Phys,* **21,** 123-35. [pages 51,61]

Cheng, J. C. H., Wu, J. K., Huang, C. M., Liu, H. S., Huang, D. Y., Cheng, S. H., Tsai, S. Y., Jian, J. J. M., Lin, Y. M., Cheng, T. I., Horng, C. F. and Huang, A. T. (2002) *International Journal of Radiation Oncology Biology Physics,* **54,** 156-162. [page 61]

Collet, D. (1991) *Modelling binary data,* Chapman & Hall. [page 38]

Dale, R. G. (1989a) *British Journal of Radiology,* **62,** 241-244. [pages 15, 33, 34]

Dale, R. G. (1989b) *Radiotherapy and Oncology,* **15,** 371-382. [pages 15, 33, 34]

Dawson, L. A., Normolle, D., Balter, J. M., McGinn, C. J., Lawrence, T. S. and Ten Haken, R. K. (2002) *International Journal of Radiation Oncology Biology Physics,* **53,** 810-821. [page 61]

Dirac, P. M. A. (1930) *Proc. Camb. Phil. Soc.,* **26,** 361. [page 5]

Dritschilo, A., Chaffey, J. T., Bloomer, W. D. and Marck, A. (1978) *Br J Radiol,* **51,** 370-4. [page 20]

Eisbruch, A., Ten Haken, R. K., Kim, H. M., Marsh, L. H. and Ship, J. A. (1999) *Int J Radiat Oncol Biol Phys,* **45,** 577-87. [page 61]

Elkind, M. M. and Sutton, H. (1960) *Radiation Research,* **13,** 556-593. [page 13]

Emami, B., Lyman, J., Brown, A., Coia, L., Goitein, M., Munzenrider, J. E., Shank, B., Solin, L. J. and Wesson, M. (1991) *Int J Radiat Oncol Biol Phys,* **21,** 109-22. [pages 51,52, 82]

Fischer, J. J. (1969) *Br J Radiol,* **42,** 925-30. [pages 15, 33]

Fischer, J. J. and Moulder, J. E. (1975) *Radiology,* **117,** 179-84. [pages 15, 33, 36, 37, 39, 46]

Goitein, M. (1976) *Clin Radiol,* **27,** 389-404. [page 20]

Goitein M, Niemierko A and P., O. (1995) In *19th L H Gray Conference: Quantitative Imaging in Oncology.*Newcastle, UK, pp. 25-39. [pages 15, 33]

Hanin, L. G., Zaider, M. and Yakovlev, A. Y. (2001) *Int J Radiat Biol,* **77,** 205-13. [page 34]

Hendry, J. H. and Thames, H. D. (1986) *Br J Radiol,* **59,** 628-30. [page 20]

Herring, D. F. (1980) *Int. J. Radiat. Oncol. Biol. Phys.,* **6,** 225-32. [page 20]

Jackson, A., Kutcher, G. J. and Yorke, E. D. (1993) *Med Phys,* **20,** 613-25. [pages 20, 21, 24]

Jackson, A., Ten Haken, R. K., Robertson, J. M., Kessler, M. L., Kutcher, G. J. and Lawrence, T. S. (1995) *Int J Radiat Oncol Biol Phys,* **31,** 883-91. [page 38]

Kallman, P., Agren, A. and Brahme, A. (1992) *Int J Radiat Biol,* **62,** 249-62. [pages 15, 33]

Kendal, W. S. (1998) *International Journal of Radiation Biology,* **73,** 207-210. [page 34]

Kendall, D. G. (1948) *Annals of Mathematical Statistics,* **19,** 1-15. [page 18]

Kutcher, G. J. and Burman, C. (1989) *Int J Radiat Oncol Biol Phys,* **16,** 1623-30. [pages 23, 24]

Kutcher, G. J., Burman, C., Brewster, L., Goitein, M. and Mohan, R. (1991) *Int J Radiat Oncol Biol Phys,* **21,** 137-46. [pages 23, 24]

Kwa, S. L., Theuws, J. C., Wagenaar, A., Damen, E. M., Boersma, L. J., Baas, P., Muller, S. H. and Lebesque, J. V. (1998) *Radiother Oncol,* **48,** 61-9. [page 61]

Lea, D. E. (1956) *Actions of radiations on living cells,* Cambridge University Press, Cambridge, UK. [page 14]

Lea, D. E. and Catcheside, D. G. (1942) *Journal of Genetics,* **44,** 216-245. [page 14]

Lyman, J. T. (1985) *Radiat Res Suppl,* **8,** S13-9. [page 23]

Lyman, J. T. and Wolbarst, A. B. (1987) *Int J Radiat Oncol Biol Phys,* **13,** 103-9. [page 23]

Lyman, J. T. and Wolbarst, A. B. (1989) *Int J Radiat Oncol Biol Phys,* **17,** 433-6. [pages 23, 24]

Maciejewski, B., Withers, H. R., Taylor, J. M. G. and Hliniak, A. (1989) *International Journal of Radiation Oncology Biology Physics,* **16,** 831-843. [pages 15, 33, 34]

Maciejewski, B., Withers, H. R., Taylor, J. M. G. and Hliniak, A. (1990) *International Journal of Radiation Oncology Biology Physics,* **18,** 101-111. [pages 15, 33, 34]

Martel, M. K., Sahijdak, W. M., Ten Haken, R. K., Kessler, M. L. and Turrisi, A. T. (1998) *Int J Radiat Oncol Biol Phys,* **40,** 155-61. [page 61]

Moiseenko, V., Craig, T., Bezjak, A. and Van Dyk, J. (2003) *Radiotherapy and Oncology,* **67,** 265-274. [page 61]

Niemierko, A. (1997) *Med Phys,* **24,** 103-10. [pages 15, 20, 21, 33]

Niemierko, A. (1999) *Med Phys,* **26,** 1100. [page 24]

Niemierko, A. and Goitein, M. (1991) *Radiother Oncol,* **20,** 166-76. [page 24]

Niemierko, A. and Goitein, M. (1993) *Int J Radiat Oncol Biol Phys,* **25,** 135-45. [pages 21, 24]

Nilsson, P., Thames, H. D. and Joiner, M. C. (1990) *Int J Radiat Biol,* **57,** 127-42. [page 14]

Olsen, D. R., Kambestad, B. K. and Kristoffersen, D. T. (1994) *Br J Radiol,* **67,** 1218-25. [page 20]

Press, W. H., Flannery, B. P., Teukolsky, S. A. and *al., e.* (1986) *Numerical Recipes,* Cambridge University Press, Cambridge. [page 38]

Roberts, S. A. and Hendry, J. H. (1993) *Radiother Oncol,* **29,** 69-74. [pages 15, 33, 34, 38]

Roberts, S. A. and Hendry, J. H. (1998) *Int J Radiat Oncol Biol Phys,* **41,** 689-99. [pages 15, 33, 34]

Roesink, J. M., Moerland, M. A., Battermann, J. J., Hordijk, G. J. and Terhaard, C. H. J. (2001) *Int J Radiat Oncol Biol Phys,* **51,** 938-946. [page 61]

Sachs, R. K., Heidenreich, W. F. and Brenner, D. J. (1996) *Math Biosci,* **138,** 131-46. [page 18]

Schultheiss, T. E., Orton, C. G. and Peck, R. A. (1983) *Med Phys,* **10,** 410-5. [pages 20, 23]

Seppenwoolde, Y., Lebesque, J. V., de Jaeger, K., Belderbos, J. S. A., Boersma, L. J., Schilstra, C., Henning, G. T., Hayman, J. A., Martel, M. K. and Ten Haken, R. K. (2003) *International Journal of Radiation Oncology Biology Physics,* **55,** 724-735. [page 61]

Stavrev, P., Stavreva, N., Hristov, D. and Fallone, B. (2003, 24 - 29 August) In *Proc. of World Congress on Medical Physics and Biomedical Engineering*Sydney, Australia. [pages 51, 52]

Stavrev, P., Stavreva, N., Niemierko, A. and Goitein, M. (2001a) *Phys Medica,* **XVII,** 71-82. [pages 38, 51, 61]

Stavrev, P., Stavreva, N., Niemierko, A. and Goitein, M. (2001b) *Phys Med Biol,* **46,** 1501-18. [pages 24, 25]

Stavrev, P. V., Stavreva, N. A. and Round, W. H. (1997) *Australas Phys Eng Sci Med,* **20,** 4-10. [pages 15, 33]

Stavreva, N., Stavrev, P., Warkentin, B. and Fallone, B. G. (2003) *Med Phys,* **30,** 735-42. [pages 17, 19, 34-37, 39, 44, 45, 80]

Stavreva, N., Warkentin, B., Stavrev, P. and Fallone, B. G. (2005) *Med Phys,* **in print**. [pages 44, 45, 80]

Stavreva, N. A. (1997) University of Waikato, Hamilton, New Zealand. [pages 14, 36]

Stavreva, N. A., Stavrev, P. V. and Round, W. H. (1995) *Phys Med Biol,* **40,** 1735-8. [pages 15, 33]

Tarnawski, R., Widel, M. and Skladowski, K. (2003) *International Journal of Radiation Oncology Biology Physics,* **55,** 1074-1081. [pages 33-35, 37-39, 46, 80]

Taylor, J. M. G., Withers, H. R. and Mendenhall, W. M. (1990) *Radiotherapy and Oncology,* **17,** 95-102. [pages 15, 33, 34]

Thames, H. D., Bentzen, S. M., Turesson, I., Overgaard, M. and Van den Bogaert, W. (1990) *Radiother Oncol,* **19,** 219-35. [pages 15, 33, 34]

Thames, H. D., Peters, L. J. and Ang, K. K. (1989) *Front Radiat Ther Oncol,* **23,** 113-30. [pages 15, 33, 34]

Tome, W. A. and Fowler, J. F. (2000) *Int J Radiat Oncol Biol Phys,* **48,** 593-9. [pages 15, 33]

Travis, E. L. and Tucker, S. L. (1987) *International Journal of Radiation Oncology Biology Physics,* **13,** 283-287. [pages 15, 33, 34]

Tucker, S. L. and Taylor, J. M. (1996) *Int J Radiat Biol,* **70,** 539-53. [page 17]

Tucker, S. L., Thames, H. D. and Taylor, J. M. (1990) *Radiat Res,* **124,** 273-82. [pages 16, 17, 34]

Tucker, S. L. and Travis, E. L. (1990) *Radiotherapy and Oncology,* **18,** 155-163. [pages 15, 33, 34]

Vandegeijn, J. (1989) *British Journal of Radiology,* **62,** 296-298. [pages 15, 33, 34]

Vandyk, J., Mah, K. and Keane, T. J. (1989) *Radiotherapy and Oncology,* **14,** 55-69. [pages 15, 33, 34]

Wang, J. Z., Mayr, N. A., Li, X. A. and Stewart, R. D. (2005) *International Journal of Radiation Oncology Biology Physics,* **61,** 309-310. [page 80]

Webb, S. and Nahum, A. E. (1993) *Phys Med Biol,* **38,** 653-66. [pages 15, 33]

Wheldon, T. E. and Amin, A. E. (1988) *British Journal of Radiology,* **61,** 700-702. [pages 15, 33, 34]

Withers, H. R., Taylor, J. M. and Maciejewski, B. (1988a) *Int J Radiat Oncol Biol Phys,* **14,** 751-9. [page 20]

Withers, H. R., Taylor, J. M. G. and Maciejewski, B. (1988b) *Acta Oncologica,* **27,** 131-146. [pages 15, 33, 34]

Withers, H. R., Thames, H. D. and Peters, L. J. (1984) *Cancer Treat. Symp.,,* **1,** 75 -83. [page 23]

Wolbarst, A. B. (1984) *Int J Radiat Oncol Biol Phys,* **10,** 741-5. [page 20]

Wolbarst, A. B., Chin, L. M. and Svensson, G. K. (1982) *Int J Radiat Oncol Biol Phys,* **8,** 1761-9. [page 20, 21]

Wolbarst, A. B., Sternick, E. S., Curran, B. H. and Dritschilo, A. (1980) *Int J Radiat Oncol Biol Phys,* **6,** 723-8. [page 20]

Yaes, R. J. (1988) *Int J Radiat Oncol Biol Phys,* **14,** 147-57. [pages 15, 33]

Yaes, R. J. and Kalend, A. (1988) *Int J Radiat Oncol Biol Phys,* **14,** 1247-59. [page 20]

Yakovlev, A. Y. (1993) *Radiation Research,* **134,** 117-120. [page 34]

Zaider, M. and Minerbo, G. N. (2000) *Phys Med Biol,* **45,** 279-93. [pages 17, 18, 34, 35]

Zaider, M., Zelefsky, M. J., Hanin, L. G., Tsodikov, A. D., Yakovlev, A. Y. and Leibel, S. A. (2001) *Phys Med Biol,* **46,** 2745-58. [page 17, 34]

Appendix 1

The Poisson distribution arises when you count a number of events across time or over an area. It is based on four assumptions. We will use the term 'interval' to refer to either a time interval or an area, depending on the context of the problem.

1. The probability of observing a single event over a small interval is approximately proportional to the size of that interval.
2. The probability of two events occurring in the same narrow interval is negligible.
3. The probability of an event within a certain interval does not change over different intervals.
4. The probability of an event in one interval is independent of the probability of an event in any other non-overlapping interval.

Appendix 2

The MATLAB code used to fit the Tarnawski *et al* data (Ref) can be seen below.

function **fitTCPtarnawski**

```
% sets colours and shapes for points and fitted lines on graph
d0=(2:2:90)';
nc=9; % nc is the number of colonies
clr(1,:)='b+';clr(2,:)='gx';clr(3,:)='ro';

nset=3;
icell=menu('Cell Type', 'a4549', 'at478');
cell(1,:)='a4549'; cell(2,:)='at478';

% choose cell type to be considered -- 1 for a4549, 2 for at478
if (icell==1)
  load a4549s; ds=a4549s(:,1); ps = a4549s(:,2); ks=ps.*nc;
  load a4549cair; dcair=a4549cair(:,1); pcair = a4549cair(:,2); kcair=pcair.*nc;
  load a4549cr; dcr=a4549cr(:,1); pcr = a4549cr(:,2); kcr=pcr.*nc;
else
  load at478s; ds=at478s(:,1); ps = at478s(:,2); ks=ps.*nc;
  load at478cair; dcair=at478cair(:,1); pcair = at478cair(:,2); kcair=pcair.*nc;
  load at478cr; dcr=at478cr(:,1); pcr = at478cr(:,2); kcr=pcr.*nc;
end

% number of fractions in each data set
dpf=2; % dose per fraction
nfs(1:length(ds),1)=1; % number of fractions
nfcair=dcair/dpf;
nfcr=dcr/dpf;
nfs0(1:length(d0),1)=1; nfcair0=d0/dpf; nfcr0=nfcair0;

% times (days) of all fractions
Tis = 0; % acute
Ticair = FracMod(2, max(nfcair)); % cair
Ticr = FracMod(1, max(nfcr)); % cr
Tis0=Tis; Ticair0=FracMod(2,max(nfcair0)); Ticr0=FracMod(1,max(nfcr0));

% number of colonies
ns=nc; ncair=nc; ncr=nc;  % all set to common value of 9
setnos=1:3; setstr={'s','cair','cr'};

% ---------- log likelihood 'full' ----------
Lpf(3)=0;
```

```
Lpf(1) = loglike(ns,ps,ps);       deg(1)=length(ps);
Lpf(2) = loglike(ncair,pcair,pcair);  deg(2)=length(pcair);
Lpf(3) = loglike(ncr,pcr,pcr);     deg(3)=length(pcr);
degfr=sum(deg);
Lf=sum(Lpf);

cl = ['b' 'g' 'r']; % color of theoretical curves

% check initial parameters
a=.3;b=.03;lambda=0.15;Tlag=0.0; tau=2.2; N=150;
Lm=10^9; dlt=10;fixN=1;
repopin=0.0; repopout=1.0; il=0; q=0;qpre=1000;eps=0.;
% repopin refers to lambda inside LQ exponent, repopout refers to lambda outside
exponent, but as multiplier of # clonogens, which is the power of the individual
probability of death
% at most one of repopin, repopout should be = 1.0

mc1(1,:)='partial recovery & no repopulation';
mc1(2,:)='partial recovery & repopulation  ';
mc1(3,:)='full recovery & no repopulation  ';
mc1(4,:)='full recovery & repopulation     ';
mc1(5,:)='Single hit & Repopulation        ';
jcase=menu('Choose a combination',mc1(1,:),mc1(2,:),mc1(3,:),mc1(4,:),mc1(5,:));
if jcase==1 recov=1;lambda=0;
   elseif jcase==2 recov=1;
   elseif jcase==3 recov=0;lambda=0;
   elseif jcase==4 recov=0;
   elseif jcase==5 recov=0;b=0;
end
if b==0 recov=0;end; if recov==0 tau=0; end
degfr=degfr-abs(sign(a))-abs(sign(fixN))-abs(sign(b))-abs(sign(lambda))-abs(sign(Tlag))-
abs(sign(recov));

while dlt>eps il=il+1;
   q=q+1; if q>qpre tocontinue=menu([num2str(il),' iterations. Continue?'],'yes','no');
   if tocontinue==2 eps=10^9;end; q=0; end

% calculate tcp values as a function of the parameters a,b,N,lambda, Tlag
%  Zaider model --- % these are theoretical model values at dose points in data
 tcps = zaider(N,a,b,lambda,ds,nfs,Tis,tau);
 tcpcair = zaider(N,a,b,lambda,dcair,nfcair,Ticair,tau);
 tcpcr = zaider(N,a,b,lambda,dcr,nfcr,Ticr,tau);

% log likelihood method
   Lpp(3)=0;
   Lpp(1) = loglike(ns,tcps,ps);
```

```
   Lpp(2) = loglike(ncair,tcpcair,pcair);
   Lpp(3) = loglike(ncr,tcpcr,pcr);
   Lp = sum(Lpp);

% note negative sign in above Lp's -- that is why we are minimizing Lp here (instead of
maximizing
% ----------iterate values of parameters and store best values so far----------
if Lm>Lp
          dlt=abs(Lm-Lp);Lm=Lp;   bm=b;am=a;lambdam=lambda;Tlagm=Tlag;Nm=N;
taum=tau;
   tcpsm=tcps; tcpcairm=tcpcair; tcpcrm=tcpcr;
   hi=2*(+Lp-Lf); Phisq=hi2(degfr,hi,.001); % chi-squared calculations

%------------------- Plot data sets
   xld=min(d0)+2;
   figure(1);clf
   axis([0 90 0 1.00]);
   plot(ds,ps,'b+',dcair,pcair,'gx',dcr,pcr,'ro'); hold on;

   text(xld,.9,['L_{full} = -',num2str(Lf,5)]);
   text(xld,.96,['L_{max} = -',num2str(Lm,5),'; p =',num2str(Phisq,2)])
%--------------------Plotting scenarios for each of the models

   title(['N_{clon} = ',num2str(N,4),'; \alpha = ',num2str(a,3),'; \beta = ',num2str(b,4),';
\lambda= ',num2str(lambda,3),'; \tau = ',num2str(tau,3)])
   text(xld,.85,[' Zaider '])
   for ip=setnos;
       if (ip==1)
         p = zaider(N,a,b,lambda,d0,nfs0,Tis0,tau);
         p1=p;
       elseif (ip==2)
         p = zaider(N,a,b,lambda,d0,nfcair0,Ticair0,tau);
         p2=p;
       elseif (ip==3)
         p = zaider(N,a,b,lambda,d0,nfcr0,Ticr0,tau);
         p3=p;
       end
       plot(d0,p,cl(ip)); hold on;
   end
   xlabel([cell(icell,:),'. ',mc1(jcase,:),'  Dose [Gy]']);ylabel('TCP')
   drawnow
end  % end of if Lm>Lp  statement

% ---------- change parameter values using Monte Carlo (gaussian)
  tau=taum*(1+.051*randn);
```

```
  a=am*(1+.051*randn);b=bm*(1+.051*randn);
  lambda=lambdam*(1+.04*randn);
  Tlag=Tlagm*(1+.1*randn);
  N=round(Nm*(1+fixN*.1*randn));
  save test
end % end of while loop (main iteration loop)

%---------------------
function Lp = loglike(ncase, pth, pexp)
  Lp=sum(-ncase.*(pexp.*log(pth+1.e-031)+(1-pexp).*log(1-pth+1.e-031)));

%---------------------
function tcp = zaider(N,a,b,lambda,dose,nfract,Ti,tau)
   if (Ti == 0) % acute treatment
      sf = exp(-(a*dose + b*dose.^2));
      prob = (1 - sf);
   else  % one of the constant dose per fraction treatments
     % note if tau=0, no recovery is disabled
     % nfract is a vector
     nmax=max(nfract);
     dpf=max(dose)/nmax; % dpf is dose per fraction
     % calculate Ti's, survival fractions for all individual fractions up to nmax fractions
     recovsum=PartialRecCor(Ti,nmax,tau);
     % LQ survival; note the following assumes the same dose per fraction for all
     % points in a set
     i=1:nmax;
     % sf is a vector -- calculate survival after each fraction of an nmax fraction regimen
     sf = exp(-i.*(a*dpf + b*dpf^2)-2.0*recovsum.*b*dpf^2);
     % this is the sum in the denominator of Zaider TCP expression
     den=(1.0./sf(1:nmax-1)).*(exp(-lambda*Ti(2:nmax))-exp(-lambda.*Ti(1:nmax-1)));
     for i=1:length(nfract)
       densum(i)=sum(den(1:nfract(i)-1));
     end
    % now we will do calculations for each dose/nfract pair in these vectors
     num = sf(nfract) .* exp(lambda*Ti(nfract)); % vector -- numerator for each fraction
in nfract
     den2 = 1 - num.* densum;
     prob = (1 - num./den2)';
   end
   tcp=prob.^N; % tcp here is a column vector

%---------------------
function Ti=FracMod(Mod,NumFrac)
  n=NumFrac-1;
  Ti(1)=0;
  if Mod==1 % Mon - Fri 24h int i.e. conventional
```

```
    tmp=1:n;
    tmp1=sign(1-sign(mod(1:n,5)))*2;
    tmp2=cumsum(tmp1);
    Ti(2:NumFrac)=tmp+tmp2;
  elseif Mod==2
% 1 treatment every day, 7 days a week
    Ti(2:NumFrac)=1:n;
  end

%---------------------
function f=PartialRecCor(T,NumFrac,tau)
  m=NumFrac;
  f(1)=0;
  if tau==0
    f(m)=0;
  else
    for n=2:m; s=0;
      for i=2:n;for j=(i+1):(n+1);s=s+exp(- (T(j-1)-T(i-1))/tau);end;end
      f(n)=s;
    end
  end

%---------------------
function y = hi2(k,hi0,st)
hi=hi0:st:(3*(4*k));
z=exp(-hi/2).*hi.^((k-2)/2)/2^(k/2)/gamma(k/2);
y=st*sum(z);
```

Appendix 3

The repair process of irradiated cells can be mathematically represented by the following ordinary differential equation

$$\frac{dN_r}{dt} = -\frac{N_r}{\tau}$$

where N_r is the number of cells in need of repair, t is time and τ is the time proportionality coefficient. Solving the ODE produces

$$N_r(t) = N_r(0)e^{-\frac{t}{\tau}}.$$

If ΔT equals the time between two fractions of radiation, it can easily be seen that $e^{-\Delta T/\tau}$ $(= N_r(t)/N_r(0)\ )$ is the probability that no recovery occurs during this time interval ΔT, and conversely $1-e^{-\Delta T/\tau}$ is the probability of cell recovery occurring during ΔT.

By taking the simplest fractionation scheme, two fractions separated by a time ΔT, the surviving number of cells N_s is given as

$$N_s = Ne^{-\alpha(d_1+d_2)}e^{-\beta d_1^2}e^{-\beta d_2^2}\left[e^{-2\beta d_1 d_2} + (1-e^{-2\beta d_1 d_2})(1-e^{-\Delta T/\tau})\right]$$

where N is the initial number of cells before irradiation, and d_1 and d_2 are the dose given in the first and second fraction respectively. $e^{-\alpha(d_1+d_2)}e^{-\beta d_1^2}e^{-\beta d_2^2}$ is simply the probability of cell survival (using the LQ model) after doses d_1 and d_2 are delivered. $e^{-2\beta d_1 d_2}$ represents the probability that cells will survive lethal damage caused by cross-damage between doses d_1 and d_2 (dose d_1 inflicts sublethal damage that then becomes lethal damage due to dose d_2). Thus $(1-e^{-2\beta d_1 d_2})(1-e^{-\Delta T/\tau})$ is the probability of the cell

receiving lethal damage due to the cross-damage between doses d_1 and d_2, but which is repaired in the time interval ΔT (and thus the cell survives). It can readily be shown that if repair is almost instantaneous (full recovery occurs), N_s reverts to $Ne^{-\alpha D}e^{-\beta d_1^2}e^{-\beta d_2^2}$.

By using the Taylor expansion of e^{-x} for small values of x

$$e^{-x} = \sum_{n=0}^{\infty} \frac{(-x)^n}{n!} = 1 - x + \ldots ,$$

the equation $e^{-2\beta d_1 d_2} + (1 - e^{-2\beta d_1 d_2})(1 - e^{-\Delta T/\tau})$ can be shown to approach $e^{-2\beta d_1 d_2 e^{-\Delta T/\tau}}$ for small values of $2\beta d_1 d_2$.

Simplified, $e^{-2\beta d_1 d_2} + (1 - e^{-2\beta d_1 d_2})(1 - e^{-\Delta T/\tau})$ becomes $1 - e^{-\Delta T/\tau}(1 - e^{-2\beta d_1 d_2})$.

Assuming small values of $2\beta d_1 d_2$, $e^{-2\beta d_1 d_2} \cong 1 - 2\beta d_1 d_2$ or $2\beta d_1 d_2 \cong 1 - e^{-2\beta d_1 d_2}$, so the equation now becomes $1 - 2\beta d_1 d_2 e^{-\Delta T/\tau}$. As $e^{-\Delta T/\tau}$ is always lesser than or equal to 1, $2\beta d_1 d_2 e^{-\Delta T/\tau} \leq 2\beta d_1 d_2$, so the Taylor expansion can be used again and we get our final answer of $e^{-2\beta d_1 d_2 e^{-\Delta T/\tau}}$.

If N_s is then generalized for multiple fractions, it's a simple matter of multiplication of the probabilities for all possible fraction intervals. The following equation is the result, giving N_s after k fractions:

$$N_s = N \exp\left(-\alpha \sum_{i=1}^{k} d_i \right) \exp\left(-\beta \sum_{i}^{k} d_i^2 - 2\beta \sum_{i=1}^{k-1} \sum_{j=i+1}^{k} d_i d_j e^{-(T_{j-1} - T_{i-1})/\tau} \right)$$

where T_{i-1} and T_{j-1} are the times at which the i-1th and j-1th dose is delivered, respectively. Notice how $i \neq j$ as dose given by the same fraction cannot cause any cross-damage.